

---

1 Source attribution of near-surface ozone trends in the  
2 United States during 1995–2019

3  
4  
5  
6 Pengwei Li<sup>1</sup>, Yang Yang<sup>1\*</sup>, Hailong Wang<sup>2</sup>, Su Li<sup>1</sup>, Ke Li<sup>1</sup>, Pinya Wang<sup>1</sup>, Baojie  
7 Li<sup>1</sup>, Hong Liao<sup>1</sup>

8  
9  
10 <sup>1</sup>Jiangsu Key Laboratory of Atmospheric Environment Monitoring and  
11 Pollution Control, Jiangsu Collaborative Innovation Center of Atmospheric  
12 Environment and Equipment Technology, School of Environmental Science  
13 and Engineering, Nanjing University of Information Science and Technology,  
14 Nanjing, Jiangsu, China

15 <sup>2</sup>Atmospheric Sciences and Global Change Division, Pacific Northwest  
16 National Laboratory, Richland, Washington, USA

17  
18  
19  
20 \*Correspondence to yang.yang@nuist.edu.cn

---

21 **Abstract**

22 Emissions of ozone (O<sub>3</sub>) precursors in the United States have decreased  
23 in recent decades, and near-surface O<sub>3</sub> concentrations showed a significant  
24 decrease in summer but an increase in winter. In this study, an O<sub>3</sub> source  
25 tagging technique is utilized in a chemistry-climate model to investigate the  
26 source contributions to O<sub>3</sub> concentrations in the U.S. from various emitting  
27 sectors and regions of nitrogen oxides (NO<sub>x</sub>) and reactive carbon species  
28 during 1995–2019. We show that domestic emission reductions from energy  
29 and surface transportation are primarily responsible for the decrease in  
30 summertime O<sub>3</sub> during 1995–2019. However, in winter the emission control also  
31 weakens the NO<sub>x</sub> titration process, resulting in considerable increases in O<sub>3</sub>  
32 levels from natural sources. Additionally, increases in aviation and shipping  
33 activities and transpacific transport of O<sub>3</sub> from Asia largely contribute to the  
34 winter O<sub>3</sub> increase. Changes in large-scale circulation also explain 15% of the  
35 O<sub>3</sub> increasing trend.

---

## 36 1. Introduction

37 Ozone (O<sub>3</sub>) near the surface has a significant impact on air quality and  
38 public health (Haagen-Smit, 1952; Fleming et al., 2018). Since the increase in  
39 anthropogenic emissions of O<sub>3</sub> precursors from preindustrial times, O<sub>3</sub> has now  
40 become the third most important anthropogenic greenhouse gas in the  
41 troposphere (Myhre et al., 2013). Major sources of O<sub>3</sub> in the troposphere  
42 include the transport from the stratosphere and formation through  
43 photochemical reactions within the troposphere involving two chemically  
44 distinct groups of precursors: nitrogen oxides (NO<sub>x</sub>) and reactive carbon  
45 species, including carbon monoxide (CO), methane (CH<sub>4</sub>), and non-methane  
46 volatile organic compounds (NMVOCs) (Atkinson, 2000). O<sub>3</sub> precursors come  
47 from a variety of sectors, and its relatively long lifetime of about 22 days  
48 (Stevenson et al. 2006) favors the long-range transport of O<sub>3</sub>. Due to the  
49 nonlinearity of the O<sub>3</sub> production and its associated dependence on precursor  
50 emissions (Seinfeld and Pandis, 1997), attributing O<sub>3</sub> pollution to its sources is  
51 complicated.

52 Since the 1980s, O<sub>3</sub> precursor emissions have significantly reduced in the  
53 United States (Duncan et al., 2016; Xing et al., 2013; Zhang et al., 2016; Zhang  
54 et al., 2021). However, due to the nonlinear production chemistry of O<sub>3</sub>,  
55 complex seasonal meteorological influence, and long-range transport from  
56 foreign source regions, domestic emissions reductions do not imply a decrease  
57 in seasonal and annual O<sub>3</sub> concentrations. According to remote surface  
58 measurements (Cooper et al., 2020) and aircraft observations (Gaudel et al.,  
59 2020), the Sixth Assessment Report of the Intergovernmental Panel on Climate  
60 Change (Szopa et al., 2021) showed a decreasing trend in annual mean O<sub>3</sub>  
61 concentrations in the western U.S. but an increasing trend in the eastern U.S.  
62 since the mid-1990s. On the seasonal timescale, surface observations and  
63 modeling results showed that O<sub>3</sub> concentrations over the U.S. had decreased

---

64 in summer due to the reductions in domestic anthropogenic emissions and  
65 increased in winter related to the weakened NO<sub>x</sub> titration since the late 1980s  
66 (Cooper et al., 2012; Lin et al., 2017). It also shows that the increased  
67 background O<sub>3</sub>, especially due to an increased transport from Asia, can partly  
68 offset the benefit of domestic emissions control over the western U.S. in  
69 summer.

70 Source apportionment is a useful method for quantifying contributions to  
71 air pollutants from specific source regions and/or sectors, which is beneficial to  
72 emission control strategies (Yang et al., 2018). ~~The traditional~~One method of  
73 obtaining an O<sub>3</sub> source-receptor relationship is to zero out or perturb emissions  
74 from a given source region or sector in sensitivity simulations along with a  
75 baseline simulation ~~(e.g., which gives information about the response of O<sub>3</sub> to~~  
76 ~~changes in precursor emissions (e.g.,~~ Fiore et al., 2009; Hoor et al., 2009).  
77 However, emission perturbation method requires many additional model  
78 simulations when being used to estimate the contributions of multiple sources  
79 (Koo et al., 2009; Wang et al., 2014) and the perturbation method may  
80 invalidate the assumption of a linear relationship between the magnitude of the  
81 emission perturbation and the magnitude of the O<sub>3</sub> change considering the  
82 nonlinearity in O<sub>3</sub> chemistry, especially if large perturbations (e.g. zeroing out  
83 regional or sector-wide emissions) are used. The tagging approach produces  
84 information about the contribution of precursor emissions to the total amount of  
85 O<sub>3</sub>, ~~while perturbation approach gives information about the response of O<sub>3</sub> to~~  
86 ~~changes in precursor emissions (Butler et al., 2020).~~ (Butler et al., 2020). The  
87 perturbation and tagging methods are two different methods answering different  
88 scientific questions, with the first for the impacts and the last for the  
89 contributions (Grewe et al. 2010, Emmons et al. 2012, Clappier et al. 2017 and  
90 Thunis et al., 2019). Both of these two methods can be used for specific  
91 purpose to provide a comprehensive understanding source-receptor

---

92 relationships between precursor emissions and O<sub>3</sub> concentrations.

93 The source tagging method has been widely adopted in regional air quality  
94 models to examine the O<sub>3</sub> attribution in the U.S., China, and/or Europe (Collet  
95 et al., 2022; Gao et al., 2016; Lupaşcu and Butler, 2019). In some regional  
96 models, O<sub>3</sub> apportionment is based on the ratio of chemical indicators to  
97 determine the regime of O<sub>3</sub> generation (e.g., VOC-limited or NO<sub>x</sub>-limited  
98 regimes) and then attribute the generation of O<sub>3</sub> to the tag carried by a certain  
99 precursor (VOCs or NO<sub>x</sub>), which however cannot simultaneously attribute O<sub>3</sub>  
100 production to NO<sub>x</sub> and VOCs, respectively: (Dunker et al., 2002; Kwok et al.,  
101 2015), while some models do not use the chemical indicators (Lupaşcu and  
102 Butler, 2019; Mertens et al., 2020). In addition, due to the limitation in domain  
103 size of regional air quality models, they are difficult to account for contributions  
104 of intercontinental transport from several sources outside the model domain.  
105 Recently, O<sub>3</sub> tagging techniques have been implemented in the global models  
106 (e.g., Bates and Jacob, 2020; Han et al., 2018; Sudo and Akimoto, et al., 2007;  
107 Zhang et al., 2008). However, in many global models, O<sub>3</sub> is tagged by the  
108 production regions rather than the precursor emission regions, so that O<sub>3</sub> can  
109 only be attributed to the area where O<sub>3</sub> is generated, rather than the source of  
110 precursor emissions.

111 Here, based on a state-of-the-art tagging system implementation in a  
112 global chemistry–climate model, the trends of near-surface O<sub>3</sub> concentrations  
113 in the U.S. during 1995–2019 and the source attributions of the O<sub>3</sub> variations to  
114 various emission sectors and regions of NO<sub>x</sub> and reactive carbon species are  
115 investigated in this study. Mechanisms of explaining the O<sub>3</sub> trends that involve  
116 changes in anthropogenic emissions and large-scale circulations are also  
117 explored.

## 118 **2. Methods**

### 119 **2.1 Model Description**

---

120 Tropospheric O<sub>3</sub> concentrations are simulated using the Community  
121 Atmosphere Model version 4 with Chemistry (CAM4-chem) (Lamarque et al.,  
122 2012; Tilmes et al., 2015), which is the atmospheric chemistry component of  
123 the Community Earth System Model (CESM), at a horizontal resolution of 1.9°  
124 latitude by 2.5° longitude with 26 vertical levels extending to 40 km above the  
125 surface. The height of bottom layer near the surface is about 120 m and there  
126 are about 4 layers under 2 km. The model configuration uses a comprehensive  
127 tropospheric chemistry mechanism based on the Model for Ozone and Related  
128 chemical Tracers version 4 (MOZART-4) (Emmons et al., 2010), 2012). Model  
129 configurations simulate wet deposition of gas species using the Neu and  
130 Prather (2012) scheme. Dry deposition is represented following the resistance  
131 approach originally described in Wesely (1989). Stratosphere-troposphere  
132 exchange of O<sub>3</sub> is treated by setting O<sub>3</sub> to stratospheric values as their  
133 climatological means over 1996–2005 at the tropopause, ~~which~~ (Lamarque et  
134 al., 2012), which is affected by atmospheric circulation and experiences the  
135 same loss rates as O<sub>3</sub> in the troposphere (Tilmes et al., 2016). Sea surface  
136 temperatures and sea ice concentrations in our simulations are prescribed at  
137 present-day climatological conditions. ~~Model winds~~ The zonal and meridional  
138 wind fields are nudged towards the MERRA-2 (Modern Era Retrospective-  
139 Analysis for Research and Applications Version 2) reanalysis (Gelaro et al.,  
140 2017) at a 6-hourly relaxation timescale in this study to better constrain large-  
141 scale circulations by observations. The CAM4-chem performance in simulating  
142 tropospheric O<sub>3</sub> and precursors has been fully evaluated in Tilmes et al. (2015).

## 143 **2.2 Ozone Source Tagging Technique**

144 The novel O<sub>3</sub> source tagging technique implemented in the model was  
145 developed by Butler et al. (2018), which can provide a separate source  
146 apportionment of tropospheric O<sub>3</sub> to the two distinct groups of precursor  
147 emissions, i.e., NO<sub>x</sub> and reactive carbon (CO, CH<sub>4</sub> and NMVOCs). The portion

---

148 of tropospheric O<sub>3</sub> that is attributable to the stratosphere-troposphere exchange  
149 can also be quantified using this unique tagging technique. The source  
150 attribution of O<sub>3</sub> requires two separate model runs with the tagging applied to  
151 NO<sub>x</sub> and reactive carbon species, respectively. Details of the O<sub>3</sub> tagging  
152 technique are described in Butler et al. (2018).

153 In this study, near-surface O<sub>3</sub> is attributed to emission sectors and regions.  
154 Emissions from individual sectors, including agriculture (AGR), energy (ENE),  
155 industry (IND), residential, commercial and other (RCO), surface transportation  
156 (TRA), waste management (WST), international shipping (SHP) and biomass  
157 burning (BMB) emissions, as well as chemical production in the stratosphere  
158 (STR) and extra chemical production (XTR, a small amount of O<sub>3</sub> produced due  
159 to the self-reaction of OH radicals and the reactions of HO<sub>2</sub> with certain organic  
160 peroxy radicals) are tagged for both NO<sub>x</sub> and reactive carbon species. Aircraft  
161 (AIR), soil (SOIL) and lightning (LGT) sources are separately tagged for NO<sub>x</sub>  
162 emissions, while solvents (SLV) and biogenic (BIO) sources are separately  
163 tagged for NMVOCs emissions.

164 For the regional source attribution, we separately tag anthropogenic  
165 sources from Africa (AFR), Central America (CAM), Europe (EUR), Middle East  
166 (MDE), North America (NAM), East Asia (EAS), South Asia (SAS), Southeast  
167 Asia (SEA) and rest of the world (ROW) (see Fig. 1 for the region map) and  
168 natural sources (BMB, SOIL, LGT, BIO, STR and XTR). Additional tags for  
169 methane (CH<sub>4</sub>) and carbon monoxide (CO) are applied in both of the reactive  
170 carbon tagging simulations that are used to attribute O<sub>3</sub> to emission sectors and  
171 regions. We ~~did~~does not tag CH<sub>4</sub> ~~and CO~~ by individual sources and its  
172 contribution is lumped, because CH<sub>4</sub> is often considered separately from  
173 NMVOCs. It has a relative long lifetime in the troposphere and it is well mixed  
174 in the troposphere due to its exceptionally low reactivity, which can contribute  
175 to O<sub>3</sub> formation at any location in the troposphere where photochemical

---

176 conditions are favorable (Fiore et al., 2008). CO also has a longer lifetime and  
177 lower reactivity than most NMVOCs. ~~On the other hand, the number of tags is~~  
178 ~~limited by the complexity of chemical mechanism, separately tagging of CO is~~  
179 ~~more conducive to distinguish its contribution to O<sub>3</sub> from other NMVOCs.~~  
180 Therefore, the lumped total CO is separately tagged in the sector attribution  
181 simulations, but the CO is not specifically tagged in the regional attribution  
182 simulations due to the computational limit.

### 183 **2.3 Emissions and Observation**

184 The global anthropogenic emissions, including NO<sub>x</sub>, CO ~~and~~ NMVOCs,  
185 SO<sub>2</sub>, and NH<sub>3</sub>, over 1990–2019 are from the Community Emissions Data  
186 System (CEDS) version 20210205 (Hoesly et al., 2018). ~~(See Figs. S1–S3).~~  
187 Biomass burning emissions are obtained from the CMIP6 (Coupled Model  
188 Intercomparison Project Phase 6) over 1990–2014 (van Marle et al., 2017) and  
189 the emissions for the following five years (2015–2019) are interpolated from the  
190 SSP2-4.5 forcing scenario (O'Neill et al., 2016). NO<sub>x</sub> emitted from soils and  
191 biogenic NMVOCs from vegetation are prescribed as in Tilmes et al. (2015) and  
192 are kept at the present-day (2000) climatological levels during simulations.  
193 Lightning emissions of NO<sub>x</sub> are estimated ~~based on the Price using online~~  
194 ~~parameterization (Price based on simulated cloud top heights from Price et al.,~~  
195 ~~(1997), which is scaled to provide a global annual emission of 3–5 Tg N yr<sup>-1</sup>~~  
196 ~~as Lamarque et. al. (2012).~~ CH<sub>4</sub> ~~concentration~~ mixing ratio is fixed at a global  
197 average of 1750 parts per billion (ppb, volume ratio in this study) during  
198 simulations.

199 Surface O<sub>3</sub> measurements in the U.S. are obtained from the U.S.  
200 Environmental Protection Agency (EPA). Linear trends of surface O<sub>3</sub> are  
201 calculated separately for boreal summer (June-July-August, JJA) and winter  
202 (December-January-February, DJF). Seasonal mean for any site that has less  
203 than 50% data availability in any month of a season is not calculated. O<sub>3</sub> trends



---

204 at sites is shown only when the data availability is greater than 85% during the  
205 analyzed period.

### 206 **2.34 Experimental Design**

207 In this study, four groups of experiments are conducted, each group  
208 includes both NO<sub>x</sub> tagging simulation and reactive carbon tagging simulation.  
209 Two BASE experiment groups include simulations with emission sectors and  
210 regions, respectively, tagged for the two chemical distinct precursors. The  
211 BASE experiments are performed with time-varying anthropogenic emissions  
212 and winds nudged to MERRA-2 reanalysis. The other two groups of sensitivity  
213 experiments (MET) are the same as BASE experiments, except that the  
214 anthropogenic emissions are held at year 2019 level during simulations. All  
215 experiments are performed over 1990–2019, with the first 5 years treated as  
216 model spin-up and the last 25 years used for analysis. The BASE experiments  
217 are analyzed to quantify the source attributions of O<sub>3</sub> in the U.S., unless stated  
218 otherwise.

### 219 **2.5 Model Evaluation**

220 Figure S4 compares the simulated near-surface O<sub>3</sub> concentrations with  
221 those from observations in 1995 and 2019, respectively. In general, the model  
222 overestimates O<sub>3</sub> concentrations in the U.S. in both summer and winter by 10–  
223 40%. It can capture the O<sub>3</sub> seasonality that high concentrations in summer and  
224 low concentrations in winter. The spatial distributions can also be roughly  
225 captured by the model, with statistically significant correlation coefficients  
226 between simulations and observations in the range of 0.21–0.45. From 1995 to  
227 2019, the O<sub>3</sub> concentrations in the U.S. decreased in summer and increased in  
228 winter presented in observations. The model can produce the sign of the  
229 changes, but has large biases in magnitudes, which will be discussed in the  
230 following section.

231

---

## 232 3 Results

### 233 3.1 Ground-level ozone trends in the U.S.

234 Emissions of O<sub>3</sub> precursors have substantially reduced since 1995 in both  
235 the western U.S. (WUS, 100–125°W, 30–45°N) and eastern U.S. (EUS, 70–  
236 100°W, 30–45°N), primarily owing to the reductions in anthropogenic  
237 emissions (Figs. S1–S3). However, the simulated annual near-surface O<sub>3</sub>  
238 concentrations present opposite trends between WUS and EUS, with increases  
239 in EUS but weak decreases in WUS, which also exist in observations (Fig. 2a).

240 Looking at different seasons, we found the simulated contrasting trends in  
241 annual mean O<sub>3</sub> concentrations between the WUS and EUS are dominated by  
242 the strong decreases in O<sub>3</sub> concentrations in summer across the U.S. and  
243 increased O<sub>3</sub> levels in winter over the central-eastern U.S. during 1995–2019.

244 The opposite trends between summer and winter have also been noted in many  
245 previous studies (e.g., Copper et al., 2012; Lin et al., 2017, Jaffe et al., 2018).

246 ~~CAM4 Chem can well reproduce the spatial distribution of the O<sub>3</sub> trends, with~~  
247 ~~spatial correlation coefficients of 0.70 in summer and 0.92 in winter between~~  
248 ~~observed and simulated trends in the continental U.S. during 1995–2019.~~ The  
249 model reproduces the observed O<sub>3</sub> trend of  $-3.0 \pm 0.41$  ppb/decade (linear trend  
250  $\pm$  standard error) over EUS in summer ( $-3.0 \pm 0.29$  ppb/decade in model) and  
251  $2.2 \pm 0.23$  ppb/decade and roughly captures the O<sub>3</sub> trend over WUS in winter  
252 ( $3.2 \pm 0.28$  ppb/decade in model). Table S1). The decreasing trend over WUS in  
253 summer ( $-2.3 \pm 0.20$  ppb/decade in model v.s.  $-0.5 \pm 0.42$  ppb/decade in  
254 observation) and increasing trend over EUS in winter ( $6.1 \pm 0.40$  ppb/decade in  
255 model v.s.  $2.1 \pm 0.29$  ppb/decade in observation), however, are largely  
256 overestimated in the model, partly attributed to the coarse model resolution.  
257 The model also tends to overestimate the weakening of NO<sub>x</sub> titration in winter,  
258 leading to the biases. For spring and autumn, they are the transition between  
259 summer and winter, having the similar spatial pattern of O<sub>3</sub> trends as annual

---

260 average, and will not be concerned in this study.

### 261 **3.2 Source attribution of ozone trends to emission sectors**

262 During 1995–2019, summer and winter NO<sub>x</sub> emissions from energy and  
263 surface transport sectors have significantly decreased in both WUS and EUS,  
264 followed by industry and residential sectors, while those from aircraft have  
265 increased slightly (Fig. 3). Emissions of NMVOCs from surface transportation,  
266 solvents, industry, residential and waste sectors have decreased across the  
267 U.S., while those from energy and agriculture have increased. CO emissions  
268 have also significantly decreased over this time period.

269 The O<sub>3</sub> trends in the U.S. attributed to different emission source sectors  
270 are shown in Fig. 5. The time series of the source contributions from NO<sub>x</sub> and  
271 reactive carbon emissions are shown in Figs. 4, respectively. In summer, the  
272 O<sub>3</sub> attributed to energy and surface transportation NO<sub>x</sub> emissions decreased at  
273 the rate of  $2.0 \pm 0.17$  and  $1.6 \pm 0.17$  ppb/decade in WUS and  $3.2 \pm 0.15$  and  
274  $1.7 \pm 0.21$  ppb/decade in EUS, respectively (Figs. 5a and 5c). On the contrary,  
275 the O<sub>3</sub> contributed by aircraft NO<sub>x</sub> emissions increased by  $0.4 \pm 0.03$  ppb/decade  
276 in both WUS and EUS. Along with the reductions in anthropogenic emissions,  
277 natural emissions are becoming increasingly important as sources for O<sub>3</sub>  
278 formation near the surface. Although NO<sub>x</sub> emissions from soil are held at the  
279 present-day climatological levels, they account for  $0.7 \pm 0.08$  and  $1.7 \pm 0.10$   
280 ppb/decade increase in WUS and EUS, respectively, during 1995–2019, related  
281 to the changing O<sub>3</sub> production efficiency under the more NO<sub>x</sub>-sensitive  
282 condition. Note that, during 1995–2019, the molar ratio (mol N /mol C) of  
283 emitted NO<sub>x</sub> to NMVOCs reduced from 0.11 to 0.07 in the WUS and from 0.14  
284 to 0.07 in the EUS, confirming the enhanced NO<sub>x</sub>-sensitive condition during the  
285 analyzed time period. In recent decades, emissions from international shipping  
286 have increased rapidly (Eyring, 2005; Müller-Casseres et al., 2021), but have  
287 declined near the ~~increase has little impact on summer O<sub>3</sub> incoast of~~ the U.S.

---

288 ~~due~~United States. Due to a strong chemical sink associated with photolysis of  
289 O<sub>3</sub> with subsequent production of hydroxyl radical (OH) from water vapor in  
290 summer (Johnson et al., 1999), the effect of increased emissions of the far-  
291 shore ocean on the continental United States was blunted. But the increase in  
292 shipping emissions inland tends to increase O<sub>3</sub> concentrations in eastern U.S.  
293 (Fig. S5).

294 In summer, biogenic sources dominate the emissions of NMVOCs in the  
295 U.S. (Fig. S3). As the O<sub>3</sub> decreases, mainly due to the reductions in domestic  
296 NO<sub>x</sub> emissions, the contributions from biogenic emissions of NMVOCs have a  
297 decreasing trend in the U.S. during 1995–2019 (Figs. 5b and 5d), even though  
298 biogenic emissions were fixed during simulations. This also applies to CH<sub>4</sub>, of  
299 which the concentration was kept constant. This does not actually mean that  
300 CH<sub>4</sub> and biogenic NMVOCs themselves contributed to the overall O<sub>3</sub> trend  
301 through changing the precursor levels since they were kept constant during  
302 simulations; rather, ~~their O<sub>3</sub> production efficiency changed~~ mainly due to  
303 ~~changes~~the reductions in NO<sub>x</sub> emissions, O<sub>3</sub> production efficiency by reactive  
304 carbon species decreases, leading to decreasing trends of O<sub>3</sub> contribution by  
305 CH<sub>4</sub> and biogenic NMVOCs. In conjunction with NO<sub>x</sub> emission reductions,  
306 decreases in NMVOCs emissions from surface transportation and industry  
307 sectors contribute negative O<sub>3</sub> trends of  $-0.3 \pm 0.0$  and  $-0.1 \pm 0.0$  ppb/decade,  
308 respectively, in both WUS and EUS, which are offset by the increases in  
309 NMVOCs emissions from energy and agriculture sectors. Although the O<sub>3</sub>  
310 production efficiency of CO is relatively low, the contributions of CO to O<sub>3</sub>  
311 concentrations largely decreased with trends of  $-0.6 \pm 0.1$  and  $-0.5 \pm 0.1$   
312 ppb/decade in WUS and EUS, respectively, due to the massive reduction in  
313 anthropogenic emissions of CO (Fig. S1).

314 In winter, through the weakened NO<sub>x</sub> titration process (Gao et al., 2013;  
315 Simon et al., 2015), the NO<sub>x</sub> emission control causes an increase in O<sub>3</sub> levels

---

316 during 1995–2019, especially the contribution from surface transportation  
317 (0.4±0.0 ppb/decade in WUS and 0.8±0.1 ppb/decade in EUS) (Figs. 5e and  
318 5g). ~~In the context of reduced NMVOCs emissions, only~~ Although aircraft NO<sub>x</sub>  
319 emissions slightly increased, but O<sub>3</sub> attributed to aircraft NO<sub>x</sub> emissions shows  
320 positive trends as large as 0.4±0.0 and 0.6±0.0 ppb/decade in WUS and EUS,  
321 respectively. It is because aircraft emissions are injected directly into the upper  
322 troposphere and lower stratosphere in a low ambient NO<sub>x</sub> condition and have  
323 a much higher O<sub>3</sub> enhancement efficiency than surface emissions (Hodnebrog  
324 et al., 2011). ~~The increase in international shipping adds more NO<sub>x</sub> to the~~  
325 ~~polluted boundary layer environment and enhance the chemical production of~~  
326 ~~O<sub>3</sub> (Koffi et al., 2010).~~ It can be confirmed that the NO<sub>x</sub> from aircraft contributes  
327 to the increase in O<sub>3</sub> concentrations at 250 hPa in high latitude regions of the  
328 Northern Hemisphere during 1995–2019 (Fig. S6). The decrease in near-shore  
329 shipping weakened the NO<sub>x</sub> titration, together with the weakened O<sub>3</sub> chemical  
330 sink from water vapor in winter, leading to large increasing trends of O<sub>3</sub> by  
331 0.8±0.1 and 1.0±0.1 ppb/decade, respectively, in the WUS and EUS during  
332 1995–2019. Although most natural emissions do not change during the  
333 simulations, the net O<sub>3</sub> chemical production is more sensitive to NO<sub>x</sub> under the  
334 emission control condition, resulting in the increasing O<sub>3</sub> trends contributed by  
335 the soil and lightning NO<sub>x</sub> emissions. Due to the weakened NO<sub>x</sub> titration in  
336 winter, the contribution of stratospheric intrusion increases at a rate of 0.6±0.1  
337 and 1.0±0.1 ppb/decade over WUS and EUS, respectively, when stratospheric  
338 contribution to the near-surface O<sub>3</sub> ~~reaches its maximum~~ is relatively high  
339 (Butler et al., 2018). Along with the weakened NO<sub>x</sub> titration, contributions from  
340 reactive carbon emissions to the near-surface O<sub>3</sub> in the U.S. also increase for  
341 most species and sectors (Figs. 5f and 5h).

### 342 **3.3 Source attribution of ozone trends to emission regions**

343 The O<sub>3</sub> trends in the U.S. attributed to different emission source regions

---

344 are presented in Fig. 7. Time series of the source contributions are shown in  
345 Figs. 6. In summer, domestic anthropogenic NO<sub>x</sub> emissions (excluding those  
346 from soil) within North America account for 53.49% of the near-surface O<sub>3</sub>  
347 concentration averaged over the U.S. (WUS+EUS) in 1995–2019. The  
348 domestic emission reduction is the dominant factor causing the decline in  
349 surface O<sub>3</sub> concentrations, with contributions of -3.74.4±0.222 and -45.7±0.3  
350 ppb/decade to the trends over WUS and EUS, respectively, during 1995–2019  
351 (Figs. 7a and 7c). Reductions in the NMVOCs emissions from North American  
352 anthropogenic sources also decrease O<sub>3</sub> concentrations (Figs. 7b and 7d),  
353 accompanying with the domestic NO<sub>x</sub> emission control. The increase in NO<sub>x</sub>  
354 emissions from Asia contributes 0.67±0.1 ppb/decade to the total O<sub>3</sub> increasing  
355 trend in WUS, partly offsetting the negative impact of domestic emission  
356 reductions, but has a weak impact in EUS, which is consistent with previous  
357 studies (Lin et al., 2017).

358 In winter, domestic anthropogenic NO<sub>x</sub> emissions only account for 19% of  
359 the surface O<sub>3</sub> concentration in the U.S. over 1995–2019, while NO<sub>x</sub> sources  
360 from lightning, rest of the world (mainly from the international shipping), and  
361 Asia contribute 17%, 14%, and 11%, respectively, and O<sub>3</sub> from stratospheric  
362 intrusion contributes 21% of the near-surface O<sub>3</sub> in the U.S. (Fig. 6). During  
363 1995–2019, the significant increase in wintertime surface O<sub>3</sub> concentrations are  
364 not directly linked to the reductions in domestic anthropogenic emissions (Figs.  
365 7e and 7g). However, the domestic emission control weakens the NO<sub>x</sub> titration,  
366 resulting in considerable increases in O<sub>3</sub> originating from the natural sources,  
367 including O<sub>3</sub> from stratospheric intrusion, lightning and soil emissions. The  
368 natural sources combined contribute to positive O<sub>3</sub> trends of 1.42±0.2 and  
369 2.34±0.3 ppb/decade in WUS and EUS, respectively. If the O<sub>3</sub> increase is  
370 attributed to NMVOCs emissions, the combined natural source contribution is  
371 even larger (1.4±0.2 and 2.5±0.2 ppb/decade) (Figs. 7f and 7h). O<sub>3</sub> produced

---

372 by CH<sub>4</sub> increases at rates of 1.3±0.1 and 2.1±0.1 ppb/decade in WUS and EUS,  
373 respectively, due to the weakened NO<sub>x</sub> titration. Increases in aviation and  
374 shipping emissions explain the 1.2±0.1 and 1.5±0.1 ppb/decade of O<sub>3</sub> trends in  
375 WUS and EUS, respectively (Figs. 5e and 5g). Long-range transport of O<sub>3</sub>  
376 produced from Asian NO<sub>x</sub> emissions enhances the wintertime O<sub>3</sub> increasing  
377 trends by 0.9±0.1 and 1.2±0.1 ppb/decade in WUS and EUS, respectively,  
378 which are equally contributed by sources from East Asia, South Asia, and  
379 Southeast Asia (Figs. 7e and 7g).

### 380 **3.4. Impact of variations in large-scale circulations on ozone trends**

381 Many studies have reported that O<sub>3</sub> spatial distribution is strongly  
382 modulated by changes in large-scale circulations (e.g., Shen and Mickley, 2017;  
383 Yang et al., 2014, 2022). Based on our MET experiments with anthropogenic  
384 emissions kept unchanged, the changes in large-scale circulations show a  
385 weak influence on the U.S. O<sub>3</sub> trends in summer (Fig. 8a) but cause a significant  
386 O<sub>3</sub> rise in the central U.S. in winter (Fig. 8b). Averaged over the U.S., the near-  
387 surface O<sub>3</sub> concentration in winter increases at the rate of 0.7±0.3 ppb/decade  
388 during 1995–2019 in MET experiments, accounting for 15% of the trend of  
389 4.7±0.3 ppb/decade in BASE experiments. It suggests that the variation in  
390 large-scale circulations is responsible for 15% of the increase in wintertime O<sub>3</sub>  
391 concentrations in the U.S. over 1995–2019. Variations in the circulation  
392 facilitate O<sub>3</sub> transport from upper altitudes to the surface, as well as foreign  
393 contributions from Asia, which is consistent with the finding in Lin et al. (2015).  
394 The O<sub>3</sub> increasing trend in winter over the U.S. attributing to stratospheric  
395 injection and Asian NO<sub>x</sub> emissions due to dynamics are both 0.2±0.1  
396 ppb/decade (Fig. 8e). Therefore, changes in anthropogenic emissions are the  
397 main factor affecting O<sub>3</sub> trends.

398 The changes in atmospheric circulation pattern support the above finding.  
399 Compared to 1995–1999, anomalous northerly winds locate over high latitudes

---

400 of North America in 2015–2019 (Fig. 8c), strengthening the prevailing northerly  
401 winds in winter. The strengthened winds transport O<sub>3</sub> from high-latitude remote  
402 regions (e.g., Asia) to the central U.S., causing an O<sub>3</sub> accumulation. (Fig. 8g).  
403 In addition, an anomalous subsidence also occurs over the central U.S. in  
404 2015–2019, compared to 1995–1999 (Fig. 8d), leading to an anomalous  
405 downward transport of O<sub>3</sub> from high altitudes and even stratosphere to the  
406 surface. (Figs. 8g and 8h). The horizontal and vertical transport of O<sub>3</sub> together  
407 contribute to the near-surface O<sub>3</sub> increases in winter during 1995–2019  
408 associated with the changes in large-scale circulations. The anomalous  
409 atmospheric circulation is likely linked to the location of the midlatitude jet  
410 stream, which is influenced by ENSO cycle (Lin et al., 2015).

411

#### 412 **4. Conclusions and discussions**

413 Using a global chemistry–climate model equipped with an O<sub>3</sub> source  
414 tagging technique, we examine the long-term trends and source apportionment  
415 of O<sub>3</sub> in the continental U.S. over 1995–2019 to various emission source  
416 sectors and regions in this study. This model can well capture the O<sub>3</sub> increasing  
417 trend in summer and decreasing trend over the EUS in summer and increasing  
418 trend over the WUS in winter over the U.S. during this time period, but largely  
419 overestimates the decreasing trend over WUS in summer and increasing trend  
420 over EUS in winter.

421 In summer, our simulation results show that the decline in surface O<sub>3</sub> is  
422 dominated by the rapid reductions in NO<sub>x</sub> emissions from energy and surface  
423 transportation sectors, contributing to O<sub>3</sub> decreases at a rate of –2.0 and –1.6  
424 ppb/decade in WUS and –3.2 and –1.7 ppb/decade in EUS, respectively. As  
425 the anthropogenic NO<sub>x</sub> decreases, the more NO<sub>x</sub>-sensitive condition leads to a  
426 positive O<sub>3</sub> trend of 0.7 and 1.7 ppb/decade in WUS and EUS, respectively,  
427 contributed by the NO<sub>x</sub> emissions from soil. Due to the reductions in NO<sub>x</sub>



---

428 emissions, the O<sub>3</sub> production efficiency by reactive carbon species also  
429 decreased, leading to the decreasing contributions to O<sub>3</sub> from reactive carbon  
430 species ~~also decrease~~ in summer during 1995–2019. Even though biogenic  
431 NMVOCs emissions and CH<sub>4</sub> mixing ratio were fixed during simulations, their  
432 contributions also decreased related to the weakened O<sub>3</sub> production efficiency  
433 by these precursors. Source region tagging suggests that the domestic  
434 emission reductions are primarily responsible for the decreasing trend in  
435 summertime near-surface O<sub>3</sub> concentrations in the U.S. during 1995–2019.

436 The mechanisms of wintertime O<sub>3</sub> increases over the U.S. are more  
437 complex. First, the domestic emission control weakens the NO<sub>x</sub> titration,  
438 resulting in considerable increases in O<sub>3</sub> originating from natural sources,  
439 including O<sub>3</sub> from stratospheric intrusion, lightning, soil and biogenic emissions.  
440 The natural sources combined contribute a positive O<sub>3</sub> trend of more than 1 and  
441 2 ppb/decade in WUS and EUS, respectively. Second, increases in aviation and  
442 shipping emissions explain the 1.2 and 1.5 ppb/decade of O<sub>3</sub> trends in WUS  
443 and EUS, respectively. Third, long-range transport of O<sub>3</sub> produced from Asian  
444 NO<sub>x</sub> emissions enhances the wintertime O<sub>3</sub> increasing trends by 0.9 and 1.2  
445 ppb/decade in WUS and EUS, respectively. Fourth, the anomalous variation of  
446 horizontal and vertical transport ~~of~~ O<sub>3</sub> associated with the changes in large-  
447 scale circulation contributes to the near-surface O<sub>3</sub> increases over the U.S. by  
448 15% in winter during 1995–2019.

449 The overestimate of O<sub>3</sub> trend in the EUS might be related to a potential  
450 biased model representation of vertical mixing in winter. Compared to  
451 observations, the decreasing trend of O<sub>3</sub> concentrations over WUS in summer  
452 and increasing trend over EUS in winter are overestimated in the CAM4-chem  
453 model. Note that, Because most O<sub>3</sub> monitors are located in urban areas and  
454 these areas generate strong O<sub>3</sub> during the day and have strong oxidation  
455 titration at night. The, the daily and grid averaged O<sub>3</sub> concentrations output by

---

456 the model could be inconsistent with the urban observations. Besides, Lin et al.  
457 (2017) found that the contribution from increasing Asian emissions ~~offset~~  
458 that from the U.S. emission reductions, resulting in a weak O<sub>3</sub> trend in WUS. In  
459 this study, the Asian NO<sub>x</sub> emissions only contribute to 0.6 ppb/decade of the  
460 total positive trend in WUS in summer, much lower than the 3.7 ppb/decade  
461 ~~increase~~ attributable to the domestic emission reductions, suggesting  
462 that the Asian contribution to the O<sub>3</sub> trends in WUS is ~~underestimated in this~~  
463 ~~study. We also found that the model did not capture the significant increase in~~  
464 ~~summertime O<sub>3</sub> levels in China in recent years, which explains the low~~  
465 ~~contribution from Asian sources. likely underestimated in this study.~~ The bias of  
466 O<sub>3</sub> simulation in China may also lead to a bias in the wintertime O<sub>3</sub> trend over  
467 EUS. Additionally, international shipping can have a disproportionately high  
468 influence on tropospheric O<sub>3</sub> due to the dispersed nature of NO<sub>x</sub> emissions  
469 (Butler et al., (2020); Kasibhatla et al., 2000; von Glasow et al., 2003), together  
470 with the weakened NO<sub>x</sub> titration, resulting in the overestimation of O<sub>3</sub> trends.  
471 The fixed CH<sub>4</sub> ~~concentration~~ mixing ratio during simulations also biased the  
472 modeled O<sub>3</sub> trends in this study, which deserves further investigation with the  
473 varying CH<sub>4</sub> levels in future studies. The coarse model resolution also  
474 contributed to the biases. The overestimate of O<sub>3</sub> trend over EUS in winter,  
475 likely related to the bias in NO<sub>x</sub> titration, implies the overestimate of source  
476 contributions to the trends in magnitude.

477 Compared with Butler et al. (2018), the simulation in this study shares  
478 similar source sector contributions to the zonal average of O<sub>3</sub> concentrations at  
479 the surface and 400 hPa in 2010 (Figs. S7 and S8 in this study and Figs. 5 and  
480 6 in Butler et al. (2018)). The contributions from the stratosphere and lightning  
481 NO<sub>x</sub> are relatively higher in this study than Butler et al. (2018). This may be  
482 related to the different anthropogenic emission inventories used, causing  
483 different O<sub>3</sub> production/loss efficiencies by natural precursors. When comparing

---

484 the contributions from different source regions to surface O<sub>3</sub> concentrations in  
485 North America, NO<sub>x</sub> emissions from East Asia, South Asia, North America, and  
486 Europe contributed 2.2, 1.1, 8.3, and 0.7 ppb of the surface O<sub>3</sub> in North America,  
487 respectively (Fig. S9) in this study, which are also similar to those from Fig. 4 in  
488 Butler et al. (2020). Both studies show the contributions of anthropogenic  
489 NMVOCs to surface O<sub>3</sub> concentrations in North America are less than 10 ppb.

490 As the results of the study heavily depend on the emission inventory, here  
491 the potential bias in emissions are also discussed. Compared with the previous  
492 CEDS version used in this study (hereafter CEDS<sub>Hoesly</sub>), the updated CEDS  
493 inventory (hereafter CEDS<sub>GBD-MAPS</sub>) (McDuffie et al., 2020) incorporates  
494 updated activity data. For NO<sub>x</sub>, the global emission from CEDS<sub>GBD-MAPS</sub> is  
495 smaller than that of CEDS<sub>Hoesly</sub> after 2006 and shows a fast decreasing trend.  
496 By 2014, global emission of NO<sub>x</sub> is about 10 % lower than the CEDS<sub>Hoesly</sub>  
497 estimate. These differences are mainly reflected in the industrial and residential  
498 sectors in China, followed by the transportation sector in India and Africa. For  
499 global emission of NMVOCs, which remains relatively unchanged between the  
500 CEDS<sub>Hoesly</sub> and CEDS<sub>GBD-MAPS</sub> inventories (Fig. 6 in McDuffie et al. 2020). The  
501 global NO<sub>x</sub> emission from EDGAR v4.3.2 inventory is less than CEDS<sub>Hoesly</sub>  
502 (Crippa et al., 2018). This difference in NO<sub>x</sub> emissions may reduce O<sub>3</sub> trends in  
503 U.S. from foreign contributions, especially from East Asia. Recent study also  
504 reported a difference in NO<sub>x</sub> emission distribution between CMIP5 and CMIP6  
505 related to an error in data pre-processing in CEDS, leading to a northward shift  
506 of O<sub>3</sub> burden in CMIP6 (Thor et al., 2023). The aviation emissions should be  
507 corrected in future studies of O<sub>3</sub> simulations.

508

---

509 **Author contributions.** YY designed the research; PL and SL performed  
510 simulations; PL analyzed the data. All authors including HW, KL, PW, BL, and  
511 HL discussed the results and wrote the paper.

512

513 **Code and data availability.** The CESM is maintained by NCAR and is provided  
514 freely to the community. The ozone tagging code has been described by Butler  
515 et al. (2018). The MERRA-2 reanalysis data are from NASA GESDISC data  
516 (<https://goldsmr5.gesdisc.eosdis.nasa.gov/data/MERRA2/M2I6NVANA.5.12.4/>,  
517 last access: 1 August 2022). The surface O<sub>3</sub> measurements in U.S. are  
518 obtained from the U.S. Environmental Protection Agency  
519 ([https://aqs.epa.gov/aqsweb/airdata/download\\_files.html#Daily](https://aqs.epa.gov/aqsweb/airdata/download_files.html#Daily), last access: 1  
520 August 2022). The modeling results are made available at  
521 <https://doi.org/10.5281/zenodo.6891316> (last access: 1 August 2022).

522

### 523 **Acknowledgments**

524 HW acknowledges the support by the U.S. Department of Energy (DOE), Office  
525 of Science, Office of Biological and Environmental Research (BER), as part of  
526 the Earth and Environmental System Modeling program. The Pacific Northwest  
527 National Laboratory (PNNL) is operated for DOE by the Battelle Memorial  
528 Institute under contract DE-AC05-76RLO1830.

529

530 **Financial support.** This study was supported by the National Key Research  
531 and Development Program of China (grant 2020YFA0607803 and  
532 2019YFA0606800), the National Natural Science Foundation of China (grant  
533 41975159), and Jiangsu Science Fund for Distinguished Young Scholars (grant  
534 BK20211541).

535

536 **Competing interests.** The authors declare that they have no conflict of interest.

537

---

## References

- 538  
539  
540 Atkinson, R.: Atmospheric chemistry of VOCs and NO<sub>x</sub>, *Atmos. Environ.*, 34,  
541 2063-2101, [https://doi.org/10.1016/S1352-2310\(99\)00460-4](https://doi.org/10.1016/S1352-2310(99)00460-4), 2000.
- 542  
543 Bates, K. H. and Jacob, D. J.: An Expanded Definition of the Odd Oxygen  
544 Family for Tropospheric Ozone Budgets: Implications for Ozone Lifetime and  
545 Stratospheric Influence, *Geophys. Res. Lett.*, 47, e2019GL084486,  
546 <https://doi.org/10.1029/2019gl084486>, 2020.
- 547  
548 Butler, T., Lupascu, A., and Nalam, A.: Attribution of ground-level ozone to  
549 anthropogenic and natural sources of nitrogen oxides and reactive carbon in a  
550 global chemical transport model, *Atmos. Chem. Phys.*, 20, 10707-10731,  
551 <https://doi.org/10.5194/acp-20-10707-2020>, 2020.
- 552  
553 Butler, T., Lupascu, A., Coates, J., and Zhu, a. S.: TOAST 1.0: Tropospheric  
554 Ozone Attribution of Sources with Tagging for CESM 1.2.2, *Geosci. Model Dev*,  
555 <https://doi.org/10.5194/gmd-11-2825-2018>, 2018.
- 556  
557 [Castellanos, P. and Boersma, K. F.: Reductions in nitrogen oxides over Europe](https://doi.org/10.1038/srep00265)  
558 [driven by environmental policy and economic recession, \*Sci. Rep.-UK\*, 2, 265,](https://doi.org/10.1038/srep00265)  
559 <https://doi.org/10.1038/srep00265>, 2012.
- 560  
561 Collet, S., Kidokoro, T., Karamchandani, P., Jung, J., and Shah, T.: Future year  
562 ozone source attribution modeling study using CMAQ-ISAM, *J&AWMA*, 68,  
563 1239-1247 <https://doi.org/10.1080/10962247.2018.1496954>, 2018.
- 564  
565 Cooper, O. R., Gao, R.-S., Tarasick, D., Leblanc, T., and Sweeney, C.: Long-  
566 term ozone trends at rural ozone monitoring sites across the United States,  
567 1990-2010, *J. Geophys. Res.: Atmospheres*, 117, D22307,  
568 <https://doi.org/10.1029/2012JD018261>, 2012.
- 569  
570 Cooper, O. R., Schultz, M. G., Schröder, S., Chang, K.-L., Gaudel, A., Gerardo,  
571 Benítez, C., Cuevas, E., Fröhlich, M., Galbally, I. E., Kubistin, D., Lu, X., Audra,  
572 McClure-Begley, A., Molloy, S., Nédélec, P., O'Brien, J., Oltmans, S. J., Irina,  
573 Petropavlovskikh, I., Ries, L., Senik, I., Sjöberg, K., Solberg, S., Spain, T. G.,  
574 Spangl, W., Steinbacher, M., Tarasick, D., Thouret, V., and Xu, X.: Multi-decadal  
575 surface ozone trends at globally distributed remote locations, *Elem Sci Anth*, 8,  
576 23, <https://doi.org/10.1525/elementa.420>, 2020.
- 577  
578 [Clappier, A., Belis, C. A., Pernigotti, D., and Thunis, P.: Source apportionment](https://doi.org/10.5194/gmd-11-2825-2018)  
579 [and sensitivity analysis: two methodologies with two different purposes, \*Geosci.\*](https://doi.org/10.5194/gmd-11-2825-2018)

---

580 [Model Dev., 10, 4245–4256, https://doi.org/10.5194/gmd-10-4245-2017, 2017.](https://doi.org/10.5194/gmd-10-4245-2017)

581

582 [Crippa, M., Guizzardi, D., Muntean, M., Schaaf, E., Dentener, F., van Aardenne,](https://doi.org/10.5194/essd-10-1987-2018)

583 [J. A., Monni, S., Doering, U., Olivier, J. G. J., Pagliari, V., and Janssens-](https://doi.org/10.5194/essd-10-1987-2018)

584 [Maenhout, G.: Gridded emissions of air pollutants for the period 1970–2012](https://doi.org/10.5194/essd-10-1987-2018)

585 [within EDGAR v4.3.2, Earth Syst. Sci. Data, 10, 1987–2013,](https://doi.org/10.5194/essd-10-1987-2018)

586 [https://doi.org/10.5194/essd-10-1987-2018, 2018.](https://doi.org/10.5194/essd-10-1987-2018)

587

588 [de Gouw, J. A., Parrish, D. D., Frost, G. J., and Trainer, M.: Reduced emissions](https://doi.org/10.1002/2013EF000196)

589 [of CO<sub>2</sub>, NO<sub>x</sub>, and SO<sub>2</sub> from US power plants owing to switch from coal to](https://doi.org/10.1002/2013EF000196)

590 [natural gas with combined cycle technology, Earths Future, 2, 75–82,](https://doi.org/10.1002/2013EF000196)

591 [https://doi.org/10.1002/2013EF000196, 2014.](https://doi.org/10.1002/2013EF000196)

592

593 Duncan, B. N., Lamsal, L. N., Thompson, A. M., Yoshida, Y., Lu, Z., Streets, D.

594 G., Hurwitz, M. M., and Pickering, K. E.: A space-based, high-resolution view of

595 notable changes in urban NO<sub>x</sub> pollution around the world (2005–2014), J.

596 Geophys. Res., 21, 976–996, [https://doi.org/10.1002/2015JD024121, 2016.](https://doi.org/10.1002/2015JD024121)

597

598 [Duncan, B. N., Yoshida, Y., de Foy, B., Lamsal, L. N., Streets, D. G., Lu, Z.,](https://doi.org/10.1016/j.atmosenv.2013.08.068)

599 [Pickering, K. E., and Krotkov, N. A.: The observed response of Ozone](https://doi.org/10.1016/j.atmosenv.2013.08.068)

600 [Monitoring Instrument \(OMI\) NO<sub>2</sub> columns to NO<sub>x</sub> emission controls on power](https://doi.org/10.1016/j.atmosenv.2013.08.068)

601 [plants in the United States: 2005–2011, Atmos. Environ., 81, 102–111,](https://doi.org/10.1016/j.atmosenv.2013.08.068)

602 [https://doi.org/10.1016/j.atmosenv.2013.08.068, 2013.](https://doi.org/10.1016/j.atmosenv.2013.08.068)

603

604 [Dunker, A. M., Yarwood, G., Ortmann, J. P., and Wilson, G. M.: Comparison of](https://doi.org/10.1021/es011418f)

605 [Source Apportionment and Source Sensitivity of Ozone in a Three-Dimensional](https://doi.org/10.1021/es011418f)

606 [Air Quality Model, Environ. Sci. Technol., 36, 2953–2964,](https://doi.org/10.1021/es011418f)

607 [https://doi.org/10.1021/es011418f, 2002.](https://doi.org/10.1021/es011418f)

608

609 [EIA: US Energy Information Administration: Drilling Productivity Report,](https://www.eia.gov/petroleum/drilling/)

610 [available at: https://www.eia.gov/petroleum/drilling/, last access: 7 April 2020.](https://www.eia.gov/petroleum/drilling/)

611

612 [Emmons, L. K., Hess, P. G., Lamarque, J.-F., and Pfister, G. G.: Tagged ozone](https://doi.org/10.5194/gmd-5-1531-2012)

613 [mechanism for MOZART-4, CAM-chem and other chemical transport models,](https://doi.org/10.5194/gmd-5-1531-2012)

614 [Geosci. Model Dev., 5, 1531–1542, https://doi.org/10.5194/gmd-5-1531-2012,](https://doi.org/10.5194/gmd-5-1531-2012)

615 [2012.](https://doi.org/10.5194/gmd-5-1531-2012)

616

617 Emmons, L. K., Walters, S., Hess, P. G., Lamarque, J.-F., Pfister, G. G., Fillmore,

618 D., Granier, C., Guenther, A., Kinnison, D., Laepple, T., Orlando, J., Tie, X.,

619 Tyndall, G., Wiedinmyer, C., Baughcum, S. L., and Kloster, S.: Description and

620 evaluation of the Model for Ozone and Related chemical Tracers, version 4

621 (MOZART-4), Geosci. Model Dev., 3, 43–67, <https://doi.org/10.5194/gmd-3-43->

---

622 2010, 2010.  
623  
624 Eyring, V.: Emissions from international shipping: 1. The last 50 years, *J.*  
625 *Geophys. Res.*, 110, <https://doi.org/10.1029/2004JD005619>, 2005.  
626  
627 Fiore, A. M., West, J. J., Horowitz, L. W., Naik, V., and Schwarzkopf, M. D.:  
628 Characterizing the tropospheric ozone response to methane emission controls  
629 and the benefits to climate and air quality, *J. Geophys. Res.*, 113, D08307,  
630 <https://doi.org/10.1029/2007JD009162>, 2008.  
631  
632 Fiore, A. M., Dentener, F. J., Wild, O., Cuvelier, C., Schultz, M. G., Hess, P.,  
633 Textor, C., Schulz, M., Doherty, R. M., Horowitz, L. W., MacKenzie, I. A.,  
634 Sanderson, M. G., Shindell, D. T., Stevenson, D. S., Szopa, S., van Dingenen,  
635 R., Zeng, G., Atherton, C., Bergmann, D., Bey, I., Carmichael, G., Collins, W. J.,  
636 Duncan, B. N., Faluvegi, G., Folberth, G., Gauss, M., Gong, S., Hauglustaine,  
637 D., Holloway, T., Isaksen, I. S. A., Jacob, D. J., Jonson, J. E., Kaminski, J. W.,  
638 Keating, T. J., Lupu, A., Marmer, E., Montanaro, V., Park, R. J., Pitari, G., Pringle,  
639 K. J., Pyle, J. A., Schroeder, S., Vivanco, M. G., Wind, P., Wojcik, G., Wu, S.,  
640 and Zuber, A.: Multimodel estimates of intercontinental source-receptor  
641 relationships for ozone pollution, *J. Geophys. Res.*, 114, D04301 ,  
642 <https://doi.org/10.1029/2008JD010816>, 2009.  
643  
644 Fleming, Z. L., Doherty, R. M., Schneidemesser, E. V ., Malley, C. S., Cooper,  
645 O. R., Pinto, J. P ., Colette, A., Xu, X., Simpson, D., Schultz, M. G., Lefohn, A.  
646 S., Hamad, S., Moolla, R., Solberg, S., and Feng, Z.: Tropospheric Ozone  
647 Assessment Report: Present-day ozone distribution and trends relevant to  
648 human health, *Elem. Sci. Anth.*, 6, p. 12, <https://doi.org/10.1525/elementa.273>,  
649 2018.  
650  
651 Gao, J., Zhu, B., Xiao, H., Kang, H., Hou, X., and Shao, P.: A case study of  
652 surface ozone source apportionment during a high concentration episode,  
653 under frequent shifting wind conditions over the Yangtze River Delta, China, *Sci.*  
654 *Total Environ.*, 544, 853-863, <https://doi.org/10.1016/j.scitotenv.2015.12.039>,  
655 2016.Gao, Y., Fu, J. S., Drake, J. B., Lamarque, J. F., and Liu, Y.: The impact  
656 of emission and climate change on ozone in the United States under  
657 representative concentration pathways (RCPs), *Atmos. Chem. Phys.*, 13, 9607-  
658 9621, <https://doi.org/10.5194/acp-13-9607-2013>, 2013.  
659  
660 Gaudel, A., Cooper, O. R. , Chang, K. L., Bourgeois, I., Ziemke, J. R., Strode,  
661 S. A., Oman, L. D., Sellitto, P., Nédélec, P., Bolt, R., Thouret, V. and Granier,C.:  
662 Aircraft observations since the 1990s reveal increases of tropospheric ozone at  
663 multiple locations across the Northern Hemisphere, *Sci. Advance.*, 6,

---

664 <https://doi.org/10.1126/sciadv.aba8272>, 2020.

665

666 Gelaro, R., McCarty, W., Suárez, M. J., Todling, R., Molod, A., Takacs, L.,  
667 Randles, C. A., Darmenov, A., Bosilovich, M. G., Reichle, R., Wargan, K., Coy,  
668 L., Cullather, R., Draper, C., Akella, S., Buchard, V., Conaty, A., da Silva, A. M.,  
669 Gu, W., Kim, G., Koster, R., Lucchesi, R., Merkova, D., Nielsen, J. E., Partyka,  
670 G., Pawson, S., Putman, W., Rienecker, M., Schubert, S. D., Sienkiewicz, M.,  
671 and Zhao, B.: The Modern-Era Retrospective Analysis for Research and  
672 Applications, Version 2 (MERRA-2), *J. Climate*, 30, 5419–5454,  
673 <https://doi.org/10.1175/JCLI-D-16-0758.1>, 2017.

674

675 Haagen-Smit, A. J.: Chemistry and Physiology of Los Angeles Smog, *Ind. Eng.*  
676 *Chem.*, 44, 1342-1346, <https://doi.org/10.1021/ie50510a045>, 1952.

677

678 Hodnebrog, Ø., Berntsen, T. K., Dessens, O., Gauss, M., Grewe, V., Isaksen, I.  
679 S. A., Koffi, B., Myhre, G., Olivié, D., Prather, M. J., Pyle, J. A., Stordal, F., Szopa,  
680 S., Tang, Q., van Velthoven, P., Williams, J. E., and Ødemark, K.: Future impact  
681 of non-land based traffic emissions on atmospheric ozone and OH – an  
682 optimistic scenario and a possible mitigation strategy, *Atmos. Chem. Phys.*, 11,  
683 11293–11317, <https://doi.org/10.5194/acp-11-11293-2011>, 2011.

684

685 Hoesly, R. M., Smith, S. J., Feng, L., Klimont, Z., Janssens-Maenhout, G.,  
686 Pitkanen, T., Seibert, J. J., Vu, L., Andres, R. J., Bolt, R. M., Bond, T. C.,  
687 Dawidowski, L., Kholod, N., Kurokawa, J.-I., Li, M., Liu, L., Lu, Z., Moura, M. C.  
688 P., O'Rourke, P. R., and Zhang, Q.: Historical (1750–2014) anthropogenic  
689 emissions of reactive gases and aerosols from the Community Emissions Data  
690 System (CEDS), *Geosci. Model Dev.*, 11, 369–408,  
691 <https://doi.org/10.5194/gmd-11-369-2018>, 2018.

692

693 Han, H., Liu, J., Yuan, H., Zhuang, B., Zhu, Y., Wu, Y., Yan, Y., and Ding, A.:  
694 Characteristics of intercontinental transport of tropospheric ozone from Africa  
695 to Asia, *Atmos. Chem. Phys.*, 18, 4251–4276, [https://doi.org/10.5194/acp-18-](https://doi.org/10.5194/acp-18-4251-2018)  
696 [4251-2018](https://doi.org/10.5194/acp-18-4251-2018), 2018.

697

698 Hoor, P., Borken-Kleefeld, J., Caro, D., Dessens, O., Endresen, Ø., Gauss, M.,  
699 Grewe, V., Hauglustaine, D. A., Isaksen, I. S. A., Jöckel, P., Lelieveld, J., Myhre,  
700 G., Meijer, E. W., Olivié, D., Prather, M. J., Poberaj, C. S., Shine, K. P., Staehelin,  
701 J., Tang, Q., Aardenne, J. v., Velthoven, P. F. J. v., and Sausen, R.: The impact  
702 of traffic emissions on atmospheric ozone and OH: results from QUANTIFY,  
703 *Atmos. Chem. Phys.*, 9, 3113-3116, <https://doi.org/10.5194/acp-9-3113-2009>,  
704 2009.

705



---

706 Jaffe, D. A., Cooper, O. R., Fiore, A. M., Henderson, B. H., Tonnesen, G. S.,  
707 Russell, A. G., Henze, D. K., Langford, A. O., Lin, M., and Moore, T.: Scientific  
708 assessment of background ozone over the U.S.: Implications for air quality  
709 management, *Elem. Sci. Anth*, 6, 56, doi: <https://doi.org/10.1525/elementa.309>,  
710 2018.

711

712 Johnson, C., Collins, W., Stevenson, D., and Derwent, R.: Relative roles of  
713 climate and emissions changes on future tropospheric oxidant concentrations,  
714 *J. Geophys. Res.-Atmos.*, 104, 18631–18645,  
715 <https://doi.org/10.1029/1999JD900204>, 1999.

716

717 Kasibhatla, P., Levy, H., Moxim, W. J., Pandis, S. N., Corbett, J. J., Peterson,  
718 M. C., Honrath, R. E., Frost, G. J., Knapp, K., Parrish, D. D., and Ryerson, T.  
719 B.: Do emissions from ships have a significant impact on concentrations of  
720 nitrogen oxides in the marine boundary layer?, *Geophys. Res. Lett.*, 27, 2229–  
721 2232, <https://doi.org/10.1029/2000gl011387>, 2000.

722

723 ~~Koffi, B., Szopa, S., Cozic, A., Hauglustaine, D., and van Velthoven, P.: Present~~  
724 ~~and future impact of aircraft, road traffic and shipping emissions on global~~  
725 ~~tropospheric ozone, *Atmos. Chem. Phys.*, 10, 11681–11705,~~  
726 ~~<https://doi.org/10.5194/acp-10-11681-2010>, 2010.~~

727

728 Koo, B., Wilson, G. M., Morris, R., Dunker, A. M., and Yarwood, G.: Comparison  
729 of Source Apportionment and Sensitivity Analysis in a Particulate Matter Air  
730 Quality Model, *Environ. Sci. Technol.*, 43, 6669–6675,  
731 <https://doi.org/10.1021/es9008129>, 2009.

732

733 ~~Krotkov, N. A., McLinden, C. A., Li, C., Lamsal, L. N., Celarier, E. A., Marchenko,~~  
734 ~~S. V., Swartz, W. H., Bucsela, E. J., Joiner, J., Duncan, B. N., Boersma, K. F.,~~  
735 ~~Veeffkind, J. P., Levelt, P. F., Fioletov, V. E., Dickerson, R. R., He, H., Lu, Z.,~~  
736 ~~and Streets, D. G.: Aura OMI observations of regional SO<sub>2</sub> and NO<sub>2</sub> pollution~~  
737 ~~changes from 2005 to 2015, *Atmos. Chem. Phys.*, 16, 4605–4629,~~  
738 ~~<https://doi.org/10.5194/acp-16-4605-2016>, 2016.~~

739

740 ~~Kwok, R. H. F., Baker, K. R., Napelenok, S. L., and Tonnesen, G. S.:~~  
741 ~~Photochemical grid model implementation and application of VOC, NO<sub>x</sub>, and~~  
742 ~~O<sub>3</sub> source apportionment, *Geosci. Model Dev.*, 8, 99–114,~~  
743 ~~<https://doi.org/10.5194/gmd-8-99-2015>, 2015.~~

744

745 Lamarque, J.-F., Emmons, L. K., Hess, P. G., Kinnison, D. E., Tilmes, S., Vitt,  
746 F., Heald, C. L., Holland, E. A., Lauritzen, P. H., Neu, J., Orlando, J. J., Rasch,  
747 P. J., and Tyndall, G. K.: CAM-chem: description and evaluation of interactive

---

748 atmospheric chemistry in the Community Earth System Model, *Geosci. Model*  
749 *Dev.*, 5, 369–411, <https://doi.org/10.5194/gmd-5-369-2012>, 2012.

750

751 [Lin, M., Fiore, A. M., Horowitz, L. W., Langford, A. O., Oltmans, S. J., Tarasick,](#)  
752 [D., and Rieder, H. E.: Climate variability modulates western U.S. ozone air](#)  
753 [quality in spring via deep stratospheric intrusions, \*Nat. Commun.\*, 6, 7105,](#)  
754 [https://doi.org/10.1038/ncomms8105, 2015.](#)

755

756 [Lin, M., Horowitz, L. W., Payton, R., Fiore, A. M., and Tonnesen, G. S.: US](#)  
757 [surface ozone trends and extremes from 1980 to 2014: quantifying the roles of](#)  
758 [rising Asian emissions, domestic controls, wildfires, and climate, \*Atmospheric\*](#)  
759 [Chemistry and Physics, \*Atmos. Chem. Phys.\*, 17, 2943–2970,](#)  
760 [https://doi.org/10.5194/acp-17-2943-2017, 2017.](#)

761

762 [Lin, M., Fiore, A. M., Cooper, O. R., Horowitz, L. W., Langford, A. O., Levy, H.,](#)  
763 [Johnson, B. J., Naik, V., Oltmans, S. J., and Senff, C. J.: Springtime high](#)  
764 [surface ozone events over the western United States: Quantifying the role of](#)  
765 [stratospheric intrusions, \*J. Geophys. Res. Atmos.\*, 117,](#)  
766 [https://doi.org/10.1029/2012JD018151, 2012.](#)

767

768 Lupaşcu, A. and Butler, T.: Source attribution of European surface O<sub>3</sub> using a  
769 tagged O<sub>3</sub> mechanism, *Atmos. Chem. Phys.*, 19, 14535–14558,  
770 <https://doi.org/10.5194/acp-19-14535-2019>, 2019.

771

772 [Mertens, M., Kerkweg, A., Grewe, V., Jöckel, P., and Sausen, R.: Attributing](#)  
773 [ozone and its precursors to land transport emissions in Europe and Germany,](#)  
774 [Atmos. Chem. Phys., 20, 7843–7873, \[https://doi.org/10.5194/acp-20-7843-\]\(https://doi.org/10.5194/acp-20-7843-2020\)  
775 \[2020, 2020.\]\(#\)](#)

776

777 [McDuffie, E. E., Smith, S. J., O'Rourke, P., Tibrewal, K., Venkataraman, C.,](#)  
778 [Marais, E. A., Zheng, B., Crippa, M., Brauer, M., and Martin, R. V.: A global](#)  
779 [anthropogenic emission inventory of atmospheric pollutants from sector- and](#)  
780 [fuel-specific sources \(1970–2017\): an application of the Community Emissions](#)  
781 [Data System \(CEDS\), \*Earth Syst. Sci. Data\*, 12, 3413–3442,](#)  
782 [https://doi.org/10.5194/essd-12-3413-2020, 2020.](#)

783

784 Müller-Casseres, E., Edelenbosch, O. Y., Szklo, A., Schaeffer, R., and van  
785 Vuuren, D. P.: Global futures of trade impacting the challenge to decarbonize  
786 the international shipping sector, *Energy*, 237, 121547,  
787 <https://doi.org/10.1016/j.energy.2021.121547>, 2021

788

789 Myhre, G., D. Shindell, F.-M. Bréon, W. Collins, J. Fuglestedt, J. Huang, D.

---

790 Koch, J.-F. Lamarque, D. Lee, B. Mendoza, T. Nakajima, A. Robock, G.  
791 Stephens, T. Takemura and H. Zhang, 2013: Anthropogenic and Natural  
792 Radiative Forcing. In: *Climate Change 2013: The Physical Science Basis.*  
793 Contribution of Working Group I to the Fifth Assessment Report of the  
794 Intergovernmental Panel on Climate Change [Stocker, T.F., D. Qin, G.-K.  
795 Plattner, M. Tignor, S.K. Allen, J. Boschung, A. Nauels, Y. Xia, V. Bex and P.M.  
796 Midgley (eds.)]. Cambridge University Press, Cambridge, United Kingdom and  
797 New York, NY, USA, 2013.

798

799 O'Neill, B. C., Tebaldi, C., van Vuuren, D. P., Eyring, V., Friedlingstein, P., Hurtt,  
800 G., Knutti, R., Kriegler, E., Lamarque, J.-F., Lowe, J., Meehl, G. A., Moss, R.,  
801 Riahi, K., and Sanderson, B. M.: The Scenario Model Intercomparison Project  
802 (ScenarioMIP) for CMIP6, *Geosci. Model Dev.*, 9, 3461-3482,  
803 <https://doi.org/10.5194/gmd-9-3461-2016>, 2016.

804

805 Price, C., Penner, J., and Prather, M.: NO<sub>x</sub> from lightning 1, Global distribution  
806 based on lightning physics, *J. Geophys. Res.*, 102, 5929–5941,  
807 <https://doi.org/10.1029/96JD03504>, 1997.

808

809 Seinfeld, J. H. and Pandis, S. N.: *Atmospheric Chemistry and Physics: From*  
810 *Air Pollution to Climate Change*, J. Wiley, Hoboken, N.J., 2006.

811

812 Simon, H., Reff, A., Wells, B., Xing, J., and Frank, N.: Ozone trends across the  
813 United States over a period of decreasing NO<sub>x</sub> and VOC emissions, *Environ.*  
814 *Sci. Technol.*, 49, 186-195, <https://doi.org/10.1021/es504514z>, 2015.

815

816 Shen, L. and Mickley, L. J.: Effects of El Niño on summertime ozone air quality  
817 in the eastern United States *Geophys. Res. Lett.* 44, 12543–50,  
818 <https://doi.org/10.1002/2017GL076150>, 2017.

819

820 Stevenson, D. S., Dentener, F. J., Schultz, M. G., Ellingsen, K., van Noije, T. P.  
821 C., Wild, O., Zeng, G., Amann, M., Atherton, C. S., Bell, N., Bergmann, D. J.,  
822 Bey, I., Butler, T., Cofala, J., Collins, W. J., Derwent, R. G., Doherty, R. M.,  
823 Drevet, J., Eskes, H. J., Fiore, A. M., Gauss, M., Hauglustaine, D. A., Horowitz,  
824 L. W., Isaksen, I. S. A., Krol, M. C., Lamarque, J.-F., Lawrence, M. G.,  
825 Montanaro, V., Müller, J.-F., Pitari, G., Prather, M. J., Pyle, J. A., Rast, S.,  
826 Rodriguez, J. M., Sanderson, M. G., Savage, N. H., Shindell, D. T., Strahan, S.  
827 E., Sudo, K., and Szopa, S.: Multimodel ensemble simulations of present-day  
828 and near-future tropospheric ozone. *J. Geophys. Res.*, 111, D08301.  
829 <https://doi.org/10.1029/2005JD006338>, 2006.

830

831 Sudo, K., and Akimoto, H.: Global source attribution of tropospheric ozone:

---

832 Long-range transport from various source regions, *J. Geophys. Res.*, 112,  
833 D12302, <https://doi.org/10.1029/2006JD007992>, 2007.

834

835 Szopa, S., V. Naik, B. Adhikary, P. Artaxo, T. Berntsen, W.D. Collins, S. Fuzzi,  
836 L. Gallardo, A. Kiendler-Scharr, Z. Klimont, H. Liao, N. Unger, and P. Zanis:  
837 Short-Lived Climate Forcers. In *Climate Change 2021: The Physical Science*  
838 *Basis. Contribution of Working Group I to the Sixth Assessment Report of the*  
839 *Intergovernmental Panel on Climate Change* [Masson-Delmotte, V., P. Zhai,  
840 A. Pirani, S.L. Connors, C. Péan, S. Berger, N. Caud, Y. Chen, L. Goldfarb,  
841 M.I. Gomis, M. Huang, K. Leitzell, E. Lonnoy, J.B.R. Matthews, T.K.  
842 Maycock, T. Waterfield, O. Yelekçi, R. Yu, and B. Zhou (eds.)]. Cambridge  
843 University Press, Cambridge, United Kingdom and New York, NY, USA, pp.  
844 817–922, <https://doi.org/10.1017/9781009157896.008>, 2021.

845

846 [Thor, R. N., Mertens, M., Matthes, S., Righi, M., Hendricks, J., Brinkop, S., Graf,](#)  
847 [P., Grewe, V., Jöckel, P., and Smith, S.: An inconsistency in aviation emissions](#)  
848 [between CMIP5 and CMIP6 and the implications for short-lived species and](#)  
849 [their radiative forcing, \*Geosci. Model Dev.\*, 16, 1459–1466,](#)  
850 [<https://doi.org/10.5194/gmd-16-1459-2023>, 2023.](#)

851

852 [Thunis, P., Clappier, A., Tarrason, L., Cuvelier, C., Monteiro, A., Pisoni, E.,](#)  
853 [Wesseling, J., Belis, C., Pirovano, G., Janssen, S., Guerreiro, C., and Peduzzi,](#)  
854 [E.: Source apportionment to support air quality planning: Strengths and](#)  
855 [weaknesses of existing approaches, \*Environ. Int.\*, 130, 104825,](#)  
856 [<https://doi.org/10.1016/j.envint.2019.05.019>, 2019.](#)

857

858 Tilmes, S., Lamarque, J. F., Emmons, L. K., Kinnison, D. E., Marsh, D., Garcia,  
859 R. R., Smith, A. K., Neely, R. R., Conley, A., Vitt, F., Val Martin, M., Tanimoto,  
860 H., Simpson, I., Blake, D. R., and Blake, N.: Representation of the Community  
861 Earth System Model (CESM1) CAM4-chem within the Chemistry-Climate  
862 Model Initiative (CCMI), *Geosci. Model Dev.*, 9, 1853–1890,  
863 <https://doi.org/10.5194/gmd-9-1853-2016>, 2016.

864

865 Tilmes, S., Lamarque, J. F., Emmons, L. K., Kinnison, D. E., Ma, P. L., Liu, X.,  
866 Ghan, S., Bardeen, C., Arnold, S., Deeter, M., Vitt, F., Ryerson, T., Elkins, J. W.,  
867 Moore, F., Spackman, J. R., and Val Martin, M.: Description and evaluation of  
868 tropospheric chemistry and aerosols in the Community Earth System Model  
869 (CESM1.2), *Geosci. Model Dev.*, 8, 1395–1426, [https://doi.org/10.5194/gmd-8-](https://doi.org/10.5194/gmd-8-1395-2015)  
870 [1395-2015](#), 2015.

871

872 [Tilmes, S., Lamarque, J. F., Emmons, L. K., Kinnison, D. E., Ma, P. L., Liu, X.,](#)  
873 [Ghan, S., Bardeen, C., Arnold, S., Deeter, M., Vitt, F., Ryerson, T., Elkins, J. W.,](#)

---

874 [Moore, F., Spackman, J. R., and Val Martin, M.: Description and evaluation of](#)  
875 [tropospheric chemistry and aerosols in the Community Earth System Model](#)  
876 [\(CESM1.2\), Geosci. Model Dev., 8, 1395-1426, \[https://doi.org/10.5194/gmd-8-\]\(https://doi.org/10.5194/gmd-8-1395-2015\)](#)  
877 [1395-2015, 2015.](#)

878  
879 van Marle, M. J. E., Kloster, S., Magi, B. I., Marlon, J. R., Daniau, A.-L., Field,  
880 R. D., Arneth, A., Forrest, M., Hantson, S., Kehrwald, N. M., Knorr, W., Lasslop,  
881 G., Li, F., Mangeon, S., Yue, C., Kaiser, J. W., and van der Werf, G. R.: Historic  
882 global biomass burning emissions for CMIP6 (BB4CMIP) based on merging  
883 satellite observations with proxies and fire models (1750–2015), Geosci. Model  
884 Dev., 10, 3329-3357, <https://doi.org/10.5194/gmd-10-3329-2017>, 2017.

885  
886 von Glasow, R., Lawrence, M. G., Sander, R., and Crutzen, P. J.: Modeling the  
887 chemical effects of ship exhaust in the cloudfree marine boundary layer, Atmos.  
888 Chem. Phys., 3, 233–250, <https://doi.org/10.5194/acp-3-233-2003>, 2003.

889  
890 Wang, H., Rasch, P. J., Easter, R. C., Singh, B., Zhang, R., Ma, P.-L., Qian, Y.,  
891 Ghan, S. J., and Beagley, N.: Using an explicit emission tagging method in  
892 global modeling of source-receptor relationships for black carbon in the Arctic:  
893 Variations, sources, and transport pathways, J. Geophys. Res., 119, 12888-  
894 12909, <https://doi.org/10.1002/2014JD022297>, 2014.

895  
896 [Wesely, M. L.: Parameterizations for surface resistance to gaseous dry](#)  
897 [deposition in regional-scale numerical models, Atmos. Environ., 23, 1293–1304,](#)  
898 [https://doi.org/10.1016/0004-6981\(89\)90153-4, 1989.](#)

899  
900 Xing, J., Pleim, J. E., Mathur, R., Pouliot, G., Hogrefe, C., Gan, C.-M., and Wei,  
901 C.: Historical gaseous and primary aerosol emissions in the United States from  
902 1990 to 2010, Atmos. Chem. Phys., 13, 7531–7549,  
903 <https://doi.org/10.5194/acp-13-7531-2013>, 2013.

904  
905 Yang, Y., Li, M., Wang, H., Li, H., Wang, P., Li, K., Gao, M., and Liao, H.: ENSO  
906 modulation of summertime tropospheric ozone over China, Environ. Res. Lett.,  
907 17, 034020, <https://doi.org/10.1088/1748-9326/ac54cd>, 2022.

908  
909 Yang, Y., Liao, H., and Li, J.: Impacts of the East Asian summer monsoon on  
910 interannual variations of summertime surface-layer ozone concentrations over  
911 China, Atmos. Chem. Phys., 14, 6867–6879, [https://doi.org/10.5194/acp-14-](https://doi.org/10.5194/acp-14-6867-2014)  
912 [6867-2014, 2014.](#)

913  
914 Yang, Y., Wang, H., Smith, S. J., Zhang, R., Lou, S., Yu, H., Li, C., and Rasch,  
915 P. J.: Source apportionments of aerosols and their direct radiative forcing and

---

916 long-term trends over continental United States, *Earth's Future*, 6, 793–808,  
917 <https://doi.org/10.1029/2018EF000859>, 2018.  
918

919 Zhang, L., Jacob, D. J., Boersma, K. F., Jaffe, D. A., Olson, J. R., Bowman, K.  
920 W., Worden, J. R., Thompson, A. M., Avery, M. A., Cohen, R. C., Dibb, J. E.,  
921 Flock, F. M., Fuelberg, H. E., Huey, L. G., McMillan, W. W., Singh, H. B., and  
922 Weinheimer, A. J.: Transpacific transport of ozone pollution and the effect of  
923 recent Asian emission increases on air quality in North America: an integrated  
924 analysis using satellite, aircraft, ozonesonde, and surface observations, *Atmos.*  
925 *Chem. Phys.*, 8, 6117–6136, <https://doi.org/10.5194/acp-8-6117-2008>, 2008.  
926

927 Zhang, Y., Cooper, O. R., Gaudel, A., Nedelec, P., Ogino, S. Y., Thompson, A.  
928 M., and West, J. J.: Tropospheric ozone change from 1980 to 2010 dominated  
929 by equatorward redistribution of emissions, *Nat. Geosci.*, 9, 875-879,  
930 <https://doi.org/10.1038/ngeo2827>, 2016.  
931

932 Zhang, Y., West, J. J., Emmons, L. K., Flemming, J., Jonson, J. E., Lund, M. T.,  
933 Sekiya, T., Sudo, K., Gaudel, A., Chang, K. L., Nédélec, P., and Thouret, V.:  
934 Contributions of World Regions to the Global Tropospheric Ozone Burden  
935 Change From 1980 to 2010, *Geophys. Res. Lett.*, 48,  
936 <https://doi.org/10.1029/2020GL089184>, 2021.

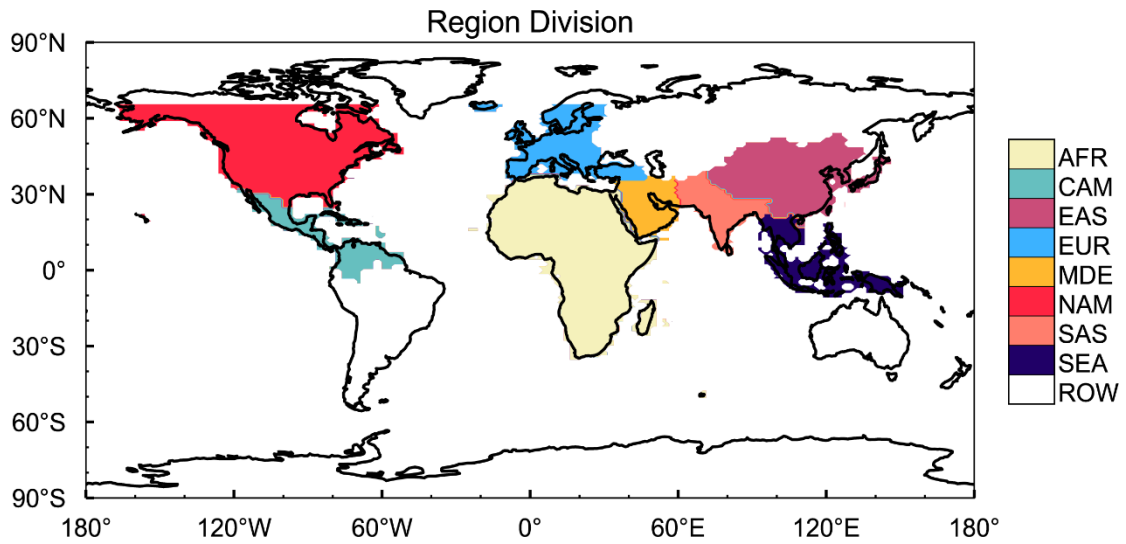
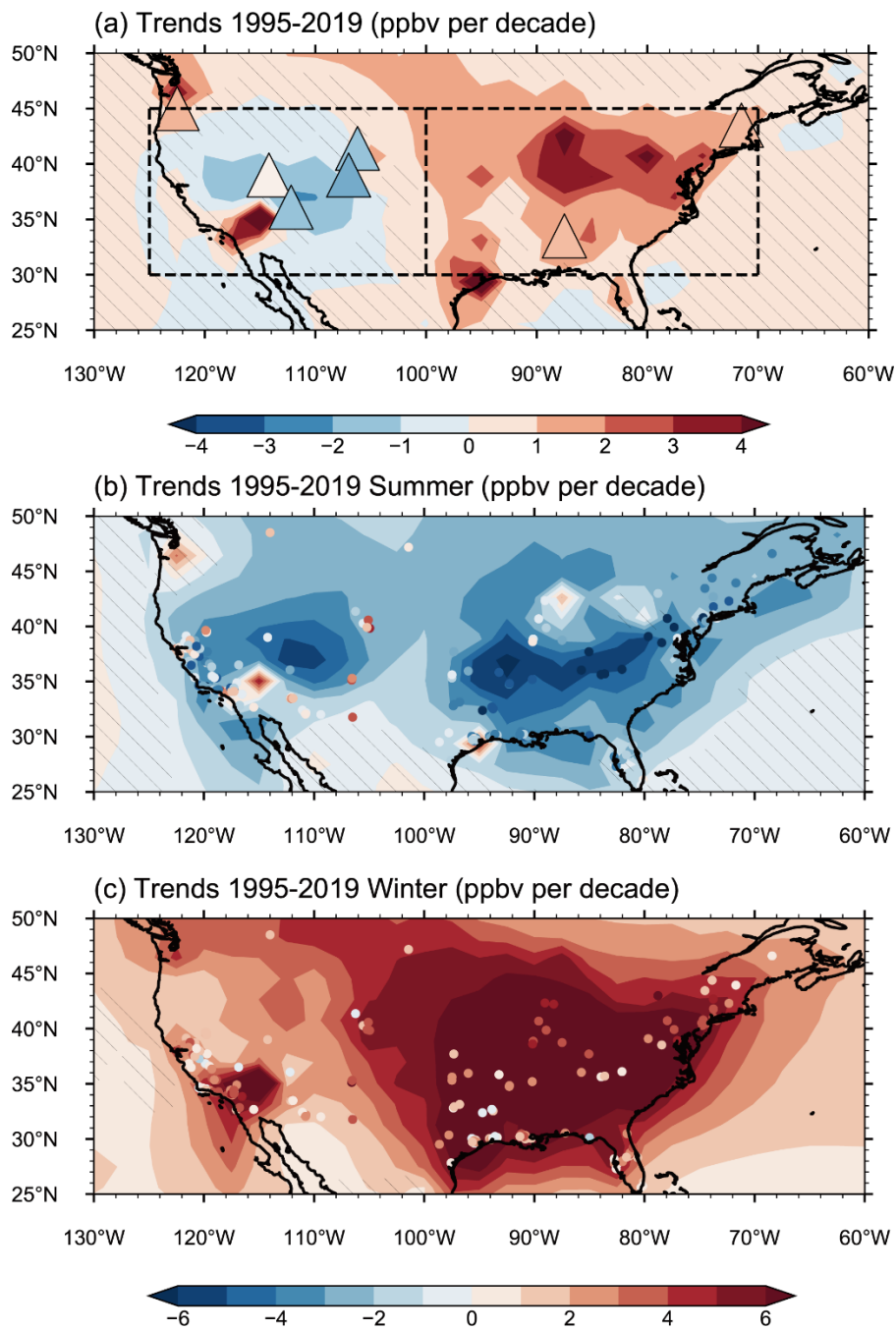


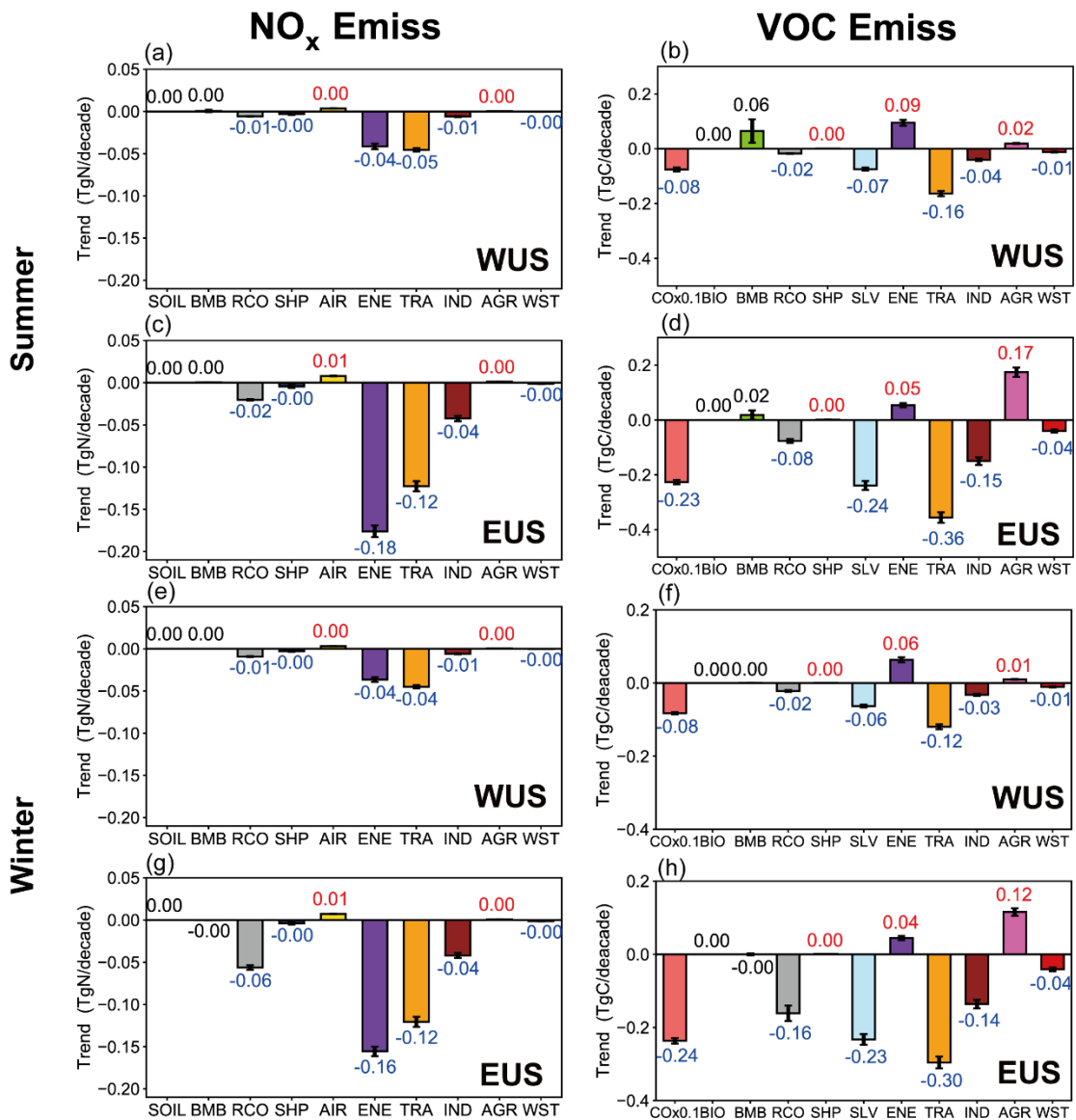
**Figure 1.** Source regions that are selected for O<sub>3</sub> source tagging in this study, include Africa (AFR), Central America (CAM), East Asia (EAS), Europe (EUR), Middle East (MDE), North America (NAM), South Asia (SAS), Southeast Asia (SEA) and rest of the world (ROW).



944  
 945  
 946  
 947  
 948  
 949  
 950  
 951  
 952  
 953  
 954  
 955

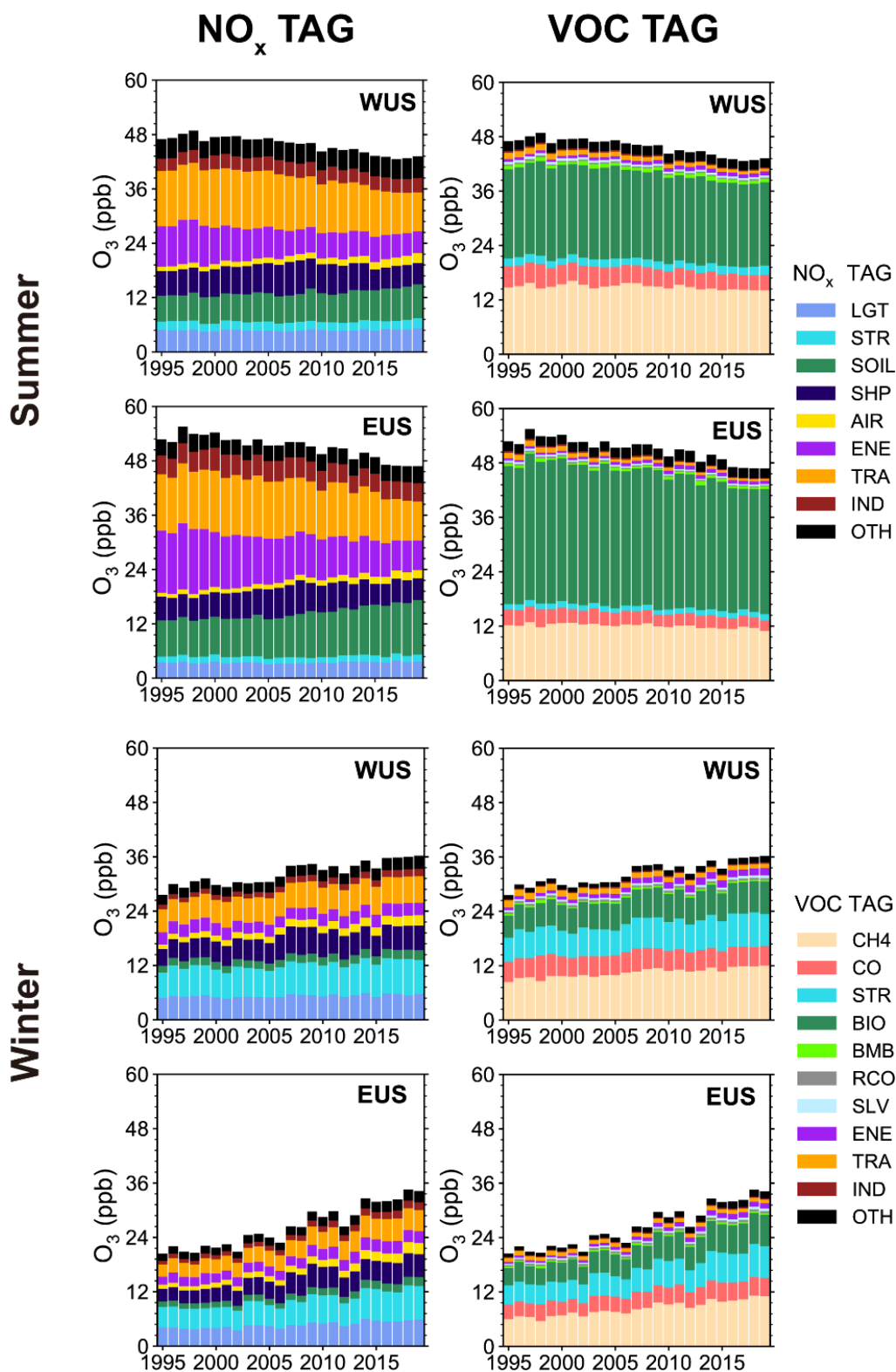
**Figure 2.** Linear trends (ppb/decade) of simulated (contours) and observed (color-filled markers) (a) annual, (b) JJA and (c) DJF mean near-surface O<sub>3</sub> concentrations during 1995–2019. Areas without hatches indicate statistical significance with 95% confidence. The boxes in (a) mark the western U.S. (WUS, 100–125°W, 30–45°N) and eastern U.S. (EUS, 70–100°W, 30–45°N), respectively. The observed annual O<sub>3</sub> concentration trends in (a) are derived from IPCC AR6, based on Cooper et al. (2020) and Gaudel et al. (2020) over 1995–2017. The observed seasonal O<sub>3</sub> concentration trends in (b) and (c) are calculated based on the U.S. EPA O<sub>3</sub> measurements over 1995–2019.





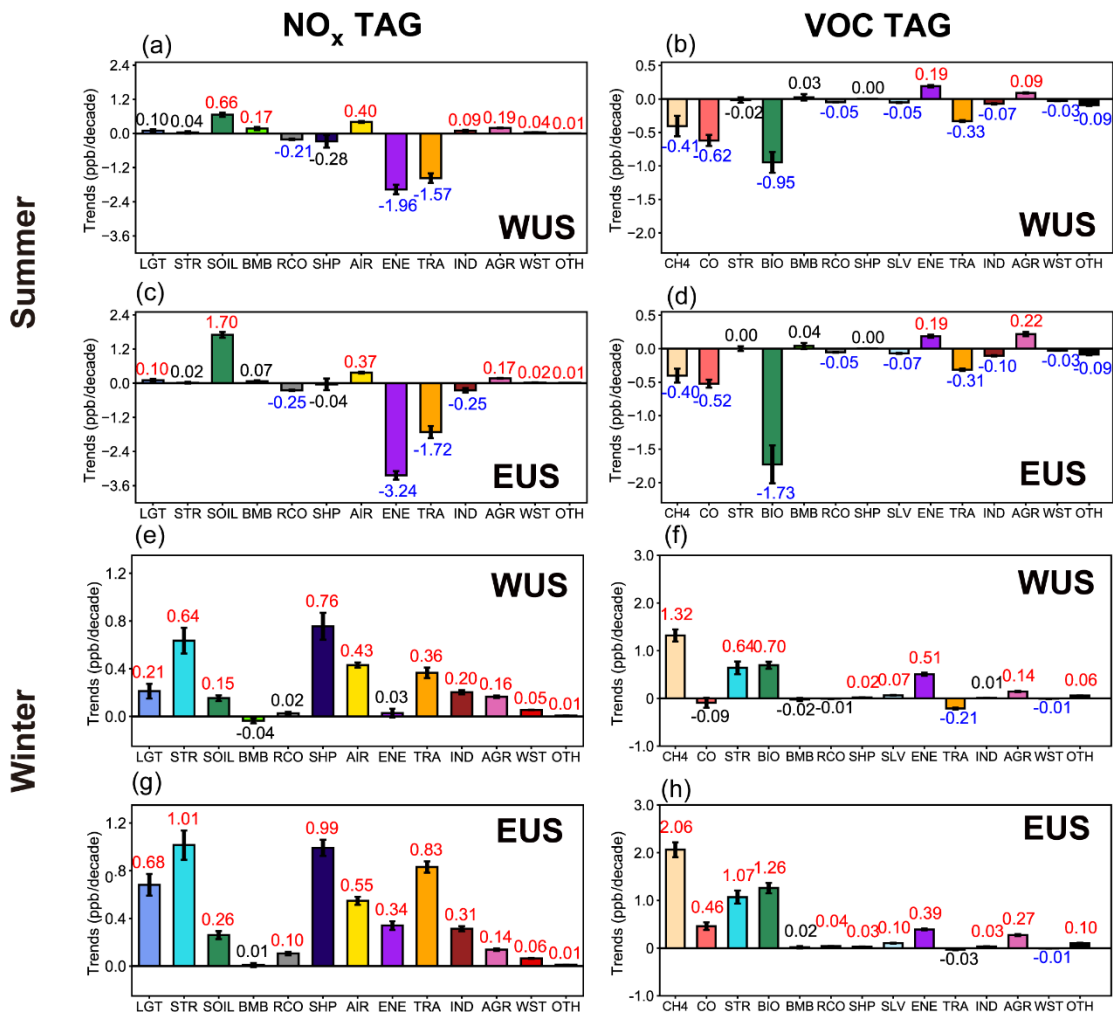
956

957 **Figure 3.** Linear trends of NO<sub>x</sub> and reactive carbon emissions from various  
 958 sectors in summer and winter over WUS and EUS. The increasing and  
 959 decreasing trends marked with red and blue values, respectively, indicate  
 960 statistical significance with 95% confidence.



961  
 962  
 963  
 964  
 965  
 966

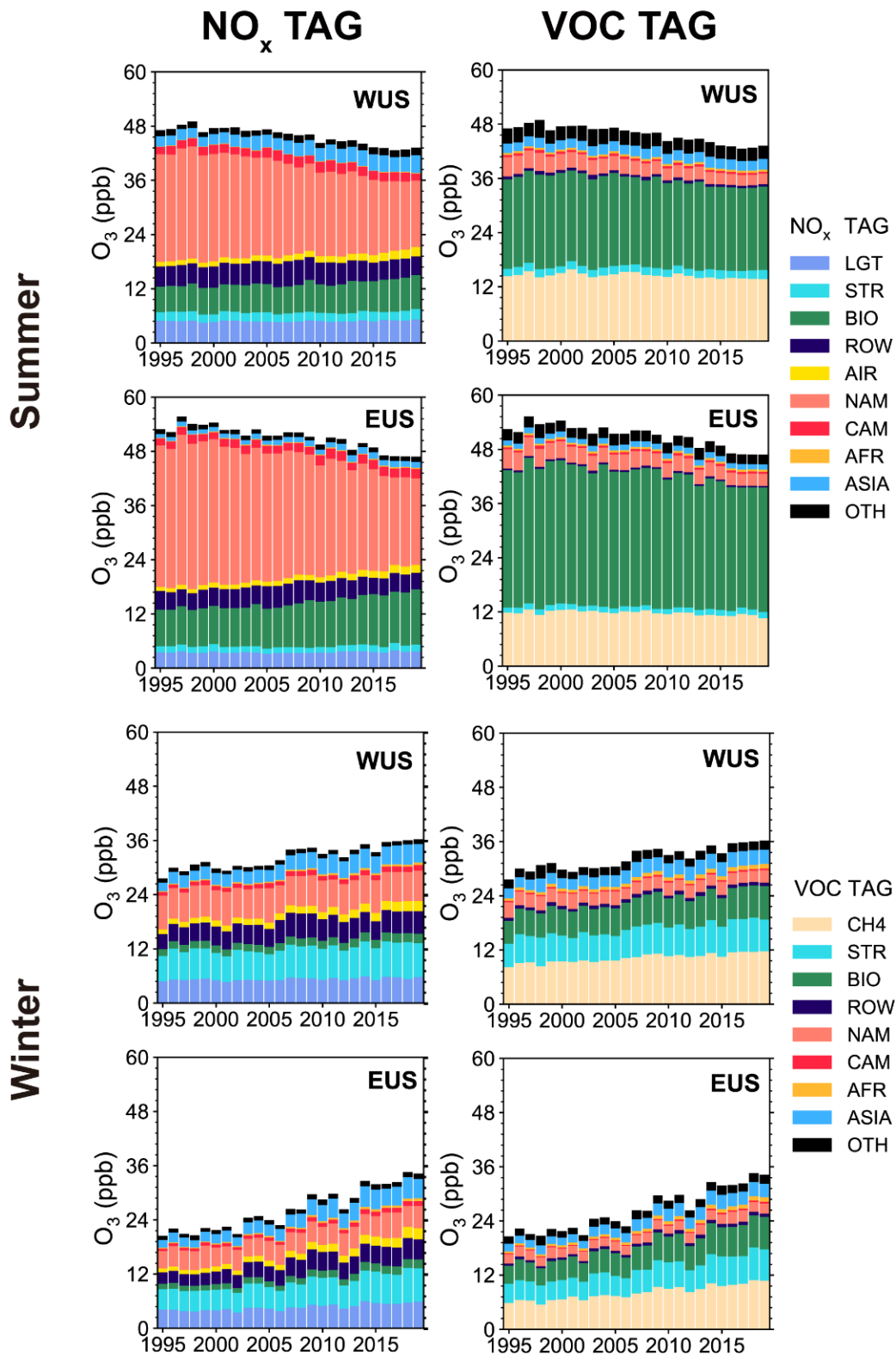
**Figure 4.** Time series of near-surface O<sub>3</sub> concentrations (ppb) averaged over WUS and EUS contributed by NO<sub>x</sub> and reactive carbon emissions from different sectors in summer and winter during 1995–2019. Sources with small contributions are combined and shown as OTH.



967

968

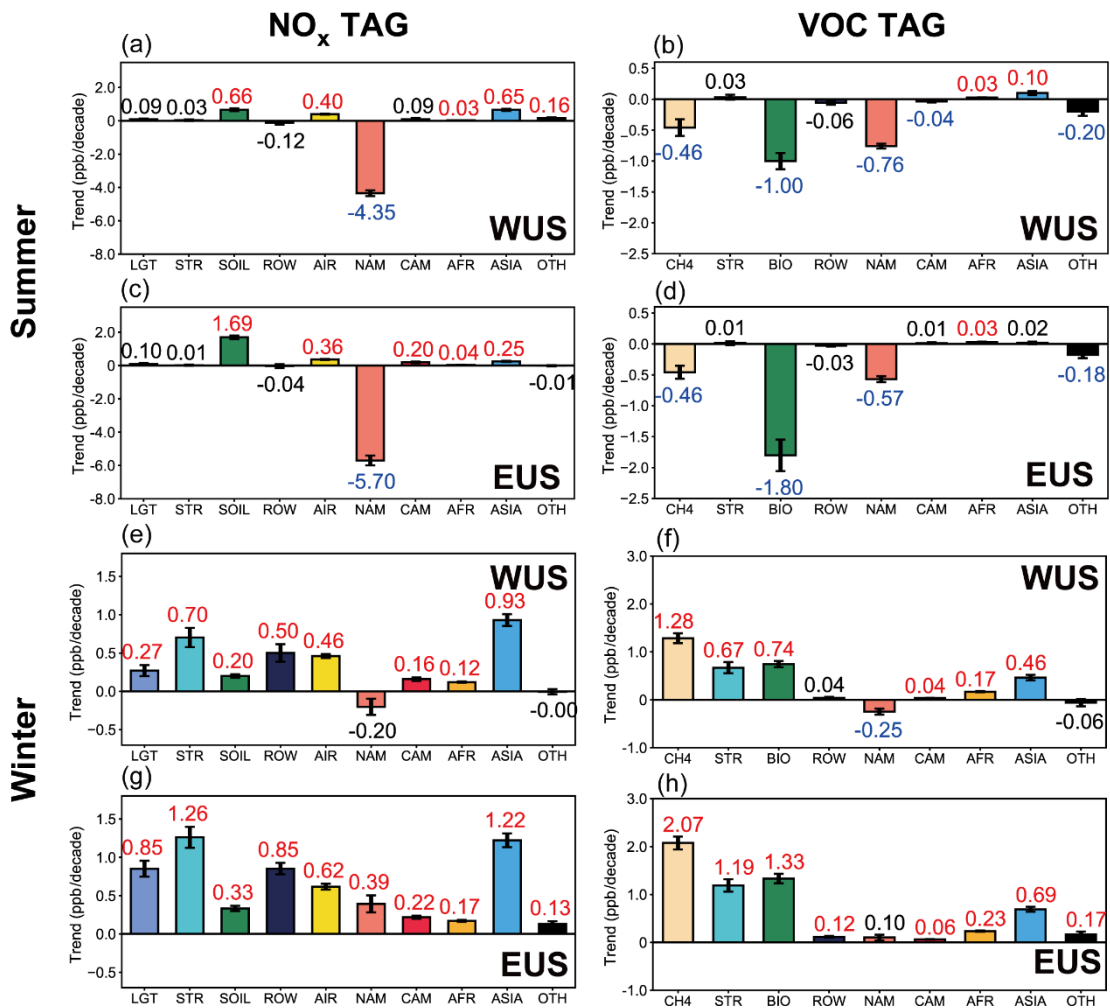
969 **Figure 5.** Linear trends (ppb/decade) of near-surface O<sub>3</sub> concentrations in  
 970 summer and winter over WUS and EUS contributed by the NO<sub>x</sub> (left) and  
 971 reactive carbon (right) emissions from various sectors (color bars). The  
 972 increasing and decreasing trends marked with red and blue color numbers,  
 973 respectively, indicate statistical significance with 95% confidence. Other  
 974 sources having small contributions are combined and shown as OTH.



975

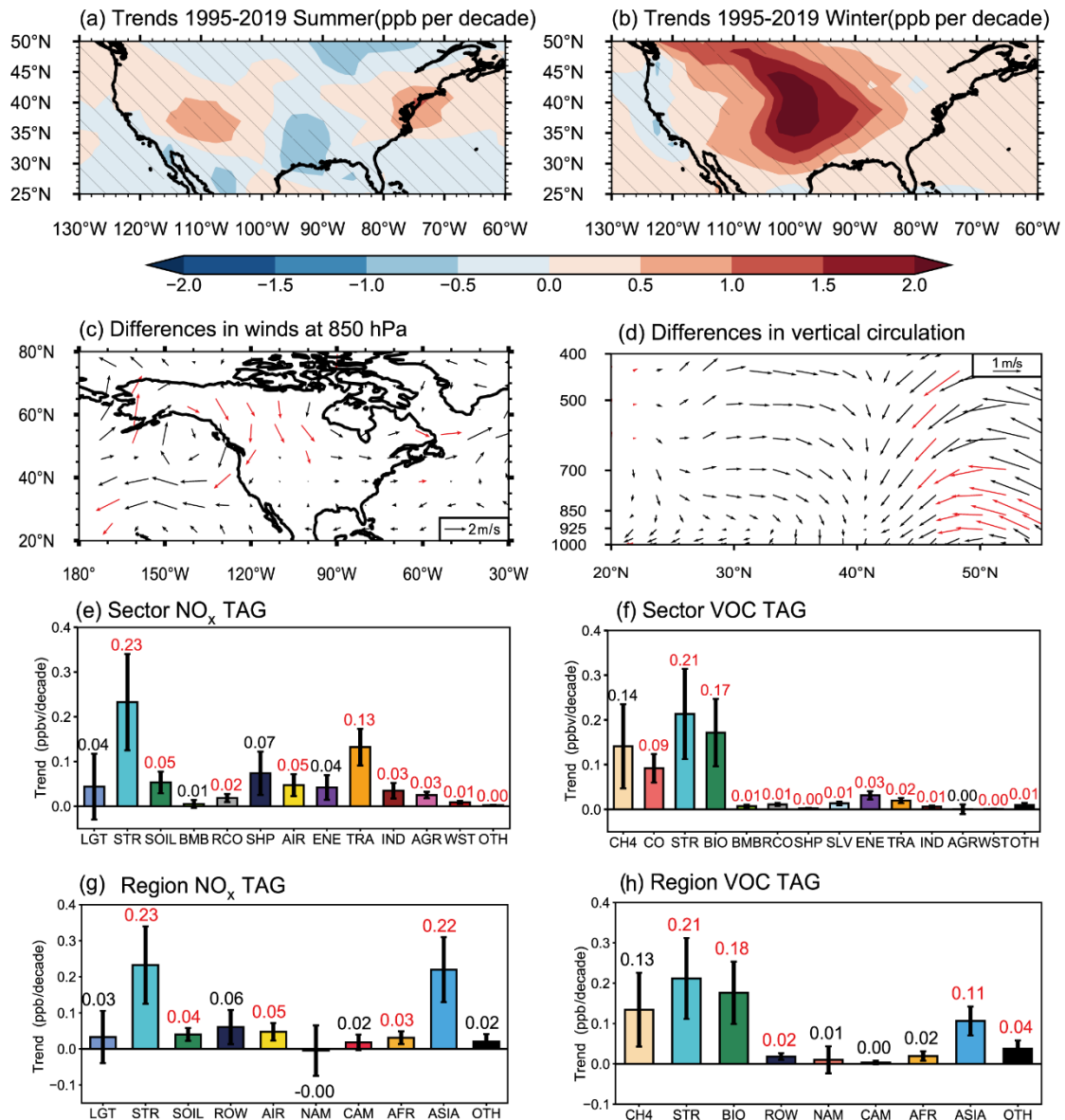
976

977 **Figure 6.** Time series of near-surface O<sub>3</sub> concentrations (ppb) averaged over  
 978 WUS and EUS contributed by NO<sub>x</sub> and reactive carbon emissions from different  
 979 source regions in summer and winter during 1995–2019. Sources with small  
 980 contributions are combined and shown as OTH.



981  
 982  
 983  
 984  
 985  
 986  
 987  
 988  
 989

**Figure 7.** Linear trends (ppb/decade) of near-surface O<sub>3</sub> concentrations in summer and winter over WUS and EUS contributed by the NO<sub>x</sub> (left) and reactive carbon (right) emissions from various source regions (color bars). The increasing and decreasing trends marked with red and blue color numbers, respectively, indicate statistical significance with 95% confidence. Contributions from source regions EAS, SAS and SEA are combined to ASIA. Other sources having small contributions are combined and shown as OTH.



990  
991

992 **Figure 8.** Linear trends (ppb/decade) of simulated (a) JJA and (b) DJF mean  
993 near-surface O<sub>3</sub> concentrations during 1995–2019. Differences between the  
994 first (1995–1999) and last (2015–2019) five years during 1995–2019 (last–  
995 first) in DJF mean (c) 850 hPa horizontal winds and (d) meridional winds and  
996 vertical velocity averaged over 90–105°W. Areas without hatches in (a) and  
997 (b) and red arrows in (c) and (d) indicate statistical significance with 95%  
998 confidence. All results are from the MET experiments. Linear trends  
999 (ppb/decade) of near-surface O<sub>3</sub> concentrations in winter over the U.S.,  
1000 contributed by the NO<sub>x</sub> (e, g) and reactive carbon (f, h) emissions from various  
1001 source sectors (e, f) and regions (g, h). The increasing and decreasing trends  
1002 marked with red and blue color numbers, respectively, indicate statistical  
1003 significance with 95% confidence. Contributions from source regions EAS,  
1004 SAS and SEA are combined to ASIA. Some sources having small  
1005 contributions are combined and shown as OTH.